A transient, perched aguifer model for banana hole formation: Evidence from San Salvador Island, Bahamas ¹Charles I. Breithaupt^{*}, ¹Jason D. Gulley, ²Eric M. Bunge, ³Paul J. Moore, ⁴Charles Kerans, ²Fermin Fernandez-Ibanez, and ² Shawn M. Fullmer ¹ School of Geosciences, University of South Florida, 4202 E Fowler Ave., Tampa, FL 33620, USA ²ExxonMobil Upstream Research Company, 22777 Springwood Village PKWY, Spring, Texas ³ ExxonMobil Upstream Integrated Solutions Company, 22777 Springwood Village PKWY, Spring, Texas 77389 ⁴ Department of Geological Sciences, and Bureau of Economic Geology, Jackson School of Geosciences, The University of Texas at Austin, USA *correspondence to: Charles I. Breithaupt, School of Geosciences, University of South Florida. E-mail: Cib@usf.edu Key words: cave, carbonates, karst, eogenetic, diagenesis, permeability, Bahamas,

Abstract

26

27

28

29

30

31

32

33

34

35

36

37

38

39

40

41

42

43

44

45

46

47

48

Banana holes are karst depressions that have primarily been reported from strandplains within the Bahamian archipelago. Banana holes have been hypothesized to form by downward dissolution in the vadose zone and in the phreatic zone by mixing dissolution and/or spatial variability in organic carbon inputs to the water table. While vadose models have been unable to explain overhanging roofs common in banana holes, phreatic models require anomalously high dissolution rates. In this study, we develop a new model for banana hole formation based on field observations, an airborne LIDAR survey, and published geochemical data on San Salvador Island, Bahamas. We detected 3356 depressions in LIDAR data consistent with banana hole morphologies in MIS 5e and MIS 9/11 strand plains. No banana holes were detected in Holocene strandplains. All banana holes were found in swales between ridges. Of the banana holes found in MIS 5e strandplains, 109 had floor elevations between 6 and 19 meters above sea level. These banana holes could not have formed in the phreatic zone because the MIS 5e freshwater lens reached a maximum elevation of 6 meters above modern sea level. We also observed banana holes filled with water during wet seasons. While wells next to banana holes were tidal, pools in the banana holes were not, indicating pools were perched. Our observations, supported by hydrological models, suggest banana holes may form in the vadose zone in transient, perched aquifers on exposure zones. Runoff from ridges infiltrates through vadose fast-flow routes until encountering low permeability exposure zones, where flow is directed laterally. Dissolution by perching on exposure zones would create thin, laterallyextensive chambers radiating from injection points. Subsequent roof collapse results in their surface expression. Because dissolution occurs when waters become perched, chambers could form throughout low stands and may therefore not reflect rapid phreatic dissolution.

Introduction

Banana holes are karst depressions which form in limestone host rock primarily in the Bahamian archipelago (Pace and Mylroie, 1993; Whitaker and Smart, 1989 Harris *et al.*, 1995; Mylroie *et al.*, 2016). Banana holes are oval to circular in plan view, usually between one and six meters deep, have width to depth ratios greater than one, are meters to tens of meters wide, and are hypothesized to form within timeframes of several hundred to a few thousand years (Harris *et al.*, 1995; Mylroie *et al.*, 2016). Unlike many karst depressions, where surface runoff creates funnel-shaped pits (Wilson and Beck, 1992; Gutierrez *et al.*, 2014), banana holes have sub-vertical to overhung walls, and often have partially to fully intact roofs (Pace and Mylroie, 1993; Harris *et al.*, 1995;). The unique morphology and abundant occurrence of banana holes in the Bahamas has led to a number of conflicting models for their formation over the last several decades.

An early model regarding banana hole formation introduced them as simple vadose dissolution pits (Whitaker and Smart, 1989). According to the vadose origin hypothesis, surficial calcretes and paleosols (Rossinsky and Wanless, 1992; Wright, 1994) funneled surface runoff to local topographic lows (Figure 1), which collected debris and plant materials. Topographic lows filled with organic rich soils, which facilitated microbial oxidation and reduction reactions that increased pCO₂ in the soil zone. Water descending though the soil zone accumulated CO₂, became undersaturated with respect to aragonite (and/or calcite) and dissolved underlying bedrock to deepen the surface pits (Figure 1) (Whitaker and Smart, 1989). Soils also promoted colonization by large rooting plants that further increased soil CO₂ and drove fracturing of the limestone. Positive feedbacks between depression deepening, focusing of runoff, soil accumulation, rooting, and dissolution resulted in biogeochemical drilling down from the land surface (Figure 1). While top-down drilling described the morphologies of some karst depressions, the hypothesis did not explain the occurrence of banana holes which have small

openings leading to large chambers and overhanging roofs. In addition, vadose processes would occur continuously during both high stand and low stand time periods, yet most banana holes extend less than 7 meters downward from the land surface indicating some vertical control on their position, or that dissolution rates are slower than previously postulated.

To address morphological conflicts with vadose hypotheses, explanations for banana hole formation shifted to phreatic models (Pace and Mylroie, 1993, Harris *et al.*, 1995; Gulley *et al.*, 2015; Mylroie *et al.*, 2016). Under phreatic models, dissolution within a freshwater lens would create isolated voids below the land surface, and subsequent collapse of thin bedrock roofs create entrances. Overhanging roofs are therefore explained by partial collapse of pre-existing voids (Figure 2).

Void formation within freshwater lenses has been suggested to result from mixing of vadose and phreatic waters at the water table (Harris *et al.*, 1995) and biogeochemical processes (Bottrell et al., 1993), possibly occurring at or near the water table (Whitaker and Smart, 1989; Whitaker and Smart, 2007; Gulley *et al.*, 2015). Mixing models suggest that dissolution occurs because the change in ion activity which governs saturation state varies by a power law while reactant concentrations of the two waters vary linearly (Plummer, 1975). As a result, calcite or aragonite undersaturation can occur even when both waters are saturated with respect to calcite or aragonite. More recent work has emphasized dissolution at water tables driven by variability in CO₂ produced near the water table (Whitaker and Smart, 2007; Gulley *et al.*, 2013, 2014 and 2016). Soil-derived organic matter transported to the water table during recharge events fuels microbial oxidation reduction reactions that drive dissolution (Bottrell *et al.*, 1993; Gulley *et al.*, 2015; Cooper *et al.*, 2016). In coastal aquifers, such oxidation-reduction processes could be further promoted by tidal fluctuation of water tables that oxygenate the vadose zone and lens top (Gulley *et al.*, 2020).

While water table models describe many of the geomorphic features observed in banana holes, some workers have suggested that other formation mechanisms more adequately describe their distributions (Mylroie et al., 2008; Mylroie et al., 2016). Firstly, voids forming at water tables should be randomly distributed, yet banana holes have been preferentially found in strandplains along trends parallel to adjacent dune ridges (Mylroie et al., 2016). Secondly, banana holes forming at water tables during MIS 5e should be found in numerous analogous settings, yet, banana holes have been reported almost exclusively in the Bahamas (Mylroie et al., 2016).

To describe the reported facies selectivity of banana holes and their dune parallel distributions, Mylroie et al. (2008 and 2016) proposed a third model for banana hole formation - mixing of fresh and saline water in prograding strandplains. Under this model, banana holes form in the fresh-saline mixing zone of the lens near the shoreline of strandplains. Locations of dissolution shift seaward as deposition and the creation of new landmass cause the mixing zone to migrate towards the ocean (Mylroie et al., 2015). Shifting in the mixing zone largely concludes void growth in the previous strandplain generation while simultaneously initiating void development at the new shoreline (Figure 3). The dune parallel trends of banana holes observed today would thus be a product of episodic void formation at prograding paleoshorefaces (Figure 3) and banana holes would essentially be immature flank margin caves (Mylroie et al., 2015). Because cave formation would be restricted to coastal mixing zones, the absence of banana holes observed in other facies such as tidal flats and lagoons is less problematic for the prograding strandplain model (Mylroie et al., 2015).

The different models for banana hole formation imply different timescales for dissolution and void development. Banana holes occur in the highest density within bedrock deposited during the last interglacial highstand, thereby limiting their formation to time periods during and after Marine isotope substage (MIS) 5e circa 124,000 -115,000 years ago (Thompson *et al.*, 2011). If

banana holes formed due to vadose processes, they could have formed at any time between the deposition of MIS 5e bedrock and the present, suggesting dissolution over 10 to 100 thousand year timescales. If banana holes formed at water tables during the MIS5e highstand, dissolution would have occurred during the narrow time window following deposition of host sediment and emplacement of a freshwater lens. In this case, dissolution would have occurred over only a portion of the 9 ka interglacial highstand after enough sediment had accumulated on the platform to create new land mass. Dissolution at the distal margin of the freshwater lens in a prograding strandplain requires the most rapid dissolution, as dissolution ceases when new land accretes and the distal margin moves seaward.

In this study, we use hydrologic, geomorphic, and geospatial data to propose a new model for the formation of banana holes that explains overhanging roofs and has more reasonable timescales for dissolution. We use a digital elevation model (DEM) derived from an airborne light detection and ranging (LiDAR) survey to investigate banana hole distributions and densities in Holocene, MIS 5e, and MIS9/11 strandplains (and foredune plains (Hesp, 2011)) on San Salvador Island, Bahamas. We evaluate the assumptions of past models by comparing banana hole distributions and abundance to topographic controls, and by investigating the potential formation of banana holes in facies other than strandplains. In addition, we use hydrological data from the most densely karstified strandplain on San Salvador to investigate the connections between pools that form in banana holes during the rainy season and the aquifer. We utilize these datasets to formulate a novel interpretation on the formation of these curious and unique landforms.

Location and Geologic Setting

San Salvador Island is an isolated carbonate platform located in the Bahamian archipelago (Figure 4). Because platform subsidence since the early Pleistocene has recently been suggested to be minimal (Godefroid *et al.*, 2019; Mylroie *et al.*, 2020), the first order

control on deposition and karstification of bedrock is glacioeustatic fluctuations in sea level (Mullins and Lynts, 1977; Mylroie and Carew, 1995; Godefroid et al., 2019) followed closely by glacioisostatic adjustments. Exposed bedrock is composed of subtidal, reef, beach and dune facies that were deposited during the Holocene, Marine isotope substage (MIS) 5a, 5e, 9, and 11 (Hearty and Kindler, 1993; Mylroie and Carew, 1995; Kerans et al., 2019a). Stratigraphic units (with the exception of the Holocene) are capped by zones of lower permeability, exposure modified bedrock which often contains one or more paleosols, breccias, or calcretes (Carew and Mylroie, 1991; Beach, 1995; Mylroie and Carew, 1995; Breithaupt, 2020). For the purposes of this manuscript, we refer to the assemblage of exposure-modified fabrics as the "exposure zone" as our primary interest is the hydrologic impact (Figure 5C). The thickest and most diagenetically mature exposure zones form in valleys where irreducible residues sourced form Saharan aerosols become embedded in carbonate laminates which form in transient ponds (Carew and Mylroie, 1991; Wright, 1994; Boardman et al., 1995). On ridges, exposure zones are thinner or non-existent because downslope mass wasting strips them from the land surface and deposits them in brecciated debris aprons at the toe of the ridge (Rossinsky and Wanless, 1992; Wright, 1994; Mylroie and Carew, 2008; Breithaupt, 2020). While exposure zones can be thin or discontinuous, they can act as aquitards (Tarbox, 1987), and have been suggested to perch lakes and wetlands (Gentry and Davis, 2006) due to their anomalously low permeabilities compared to the host limestones (Figure 5). As a result, dissolution has been suggested to occur along exposure zones in perched aquifers (Beach, 1995; Breithaupt, 2020).

148

149

150

151

152

153

154

155

156

157

158

159

160

161

162

163

164

165

166

167

168

169

170

171

172

The climate on San Salvador is semi-arid with evapotranspiration rates creating an annual water budget which is negative by ~200 mm/year (Crump and Gamble, 2006). Recharge occurs during two wet seasons from May-June, and September-November, when monthly rainfall can exceed monthly evapotranspiration. Freshwater lenses are discontinuous across the island and are concentrated within ridges in Holocene and MIS5 bedrock which have lower

permeability relative to older pre-MIS5 deposits (Breithaupt et. al, 2021). Older bedrock on the island typically contains saltwater because permeabilities are too high to support lens formation in San Salvador Island's arid climate (Vacher, 1988; Davis and Johnson, 1989; Vacher and Wallis, 1992). Measurements from monitoring wells and resistivity surveys in the Line Hole (Figure 6), Sandy Point, and Cockburntown well fields suggest the thickest lenses on the island range between 7 and 13 meters (Davis and Johnson, 1989; Kunze and Sauter, 1989; USACE, 2004).

Banana holes on San Salvador have been previously reported to occur at elevations between +1 and +7 meters relative to modern sea level (RSL), have spatial densities, by extrapolation of small surveys, of more than 1000/km² (Harris *et al.*, 1995), and are prevalent in MIS5e strandplains across San Salvador (Mylroie *et al.*, 2016). Researchers have previously measured a number of parameters for banana holes near Line Hole, Jake Jones Road, South Victoria Hill and Hard Bargain trail (Infante, 2012; Mylroie *et al.*, 2016). Surveyed banana holes in San Salvador typically range from approximately 0.5 to 7 meters in depth, have areas greater than 5 square meters, and length to width ratios less than 3 (Figure 6). Vertical dissolutional shafts known as pit caves are also reported on San Salvador (Moore and Seale, 2004; Mylroie and Carew, 2008), and typically occur in highest density at elevations above +7 meters RSL on dune ridges. The key difference between banana holes and pit caves is the width to depth ratio of banana holes is consistently greater than one, while pit caves consistently have width to depth ratios of less than one (Harris *et al.*, 1995).

Methods

Evaluating Banana Hole Size, Distribution and Abundance

To evaluate potential controls on banana hole formation we considered the size, distribution, and density of banana holes on San Salvador Island. We used a bare-earth digital elevation model to identify all depressions and used a series of morphological filters to extract

depressions fitting the description of banana holes (Figure 6). The bare earth model is derived from an aerial LiDAR survey collected and processed by the National Center for Airborne Laser Mapping (NCALM) during the summer of 2016 (Figure 4B). Raw data were processed using a static differential base station corrected in relation to the Continuous Operating Reference Station (CORS) network. The LIDAR DEM has a 0.2 meter horizontal resolution and the vertical resolution of 5-15 cm depending on the beam angle. We verified selected karst depressions observed on the LiDAR in the field during the summer of 2017, 2018, and 2019.

To collect depression metrics, we used a pattern recognition algorithm adapted from Jasiewicz and Stepinski, 2013, which defines landforms known as "geomorphons" and extracts morphometrics within polygon enclosures. Because our study is designed to capture circular to oval karst pits, we used a series of filters which excluded depressions less than ½ meter in elevation range (depth), less than 5 meters in area, and with length to width ratios greater than 3 (Figure 6). We also apply a slope filter requiring the maximum slope to be greater than 15 degrees to preclude flagging of a large number of natural enclosed depressions which form due to the natural dune morphology rather than collapse. Finally, we exclude depressions with width depth ratios >1 to avoid including pit caves in our data set (Harris *et al.*, 1995). While this method can be used to detect open pits, it cannot detect pit areas under overhangs or void areas below small entrances, and thus, some banana hole areas are inevitably underestimated or were not detected using the DEM extraction (Figure 8).

Because several locations have received nicknames which have changed over the years, we use an age and numbering convention (e.g. Holocene (H#), MIS 5e (E#), and MIS9/11 (P#)) to reference strandplains and statistical data collected therein (Table 1).

Evaluating Hydraulic Connection Between Banana Holes and the Aquifer

To evaluate the degree of connectivity between banana holes, the aquifer, and the ocean, we recorded time series of water level data in ephemeral banana hole pools (BH1 and

BH2), a deep borehole (LH-Deep: -96.5 m RSL) drilled during a past field season, the Line Hole well field (LH1, LH4, LH8, and LH13: Approx. -2 to -7 m RSL), and Grahams Harbor (Figure 7 and Table 2). We collected pressure records using HOBO U20L-04 loggers over sampling trips in July of 2015, July of 2018, and November of 2018. A 1-minute sampling interval was applied in the Line Hole wells during the first sampling trip, and a 5-minute sampling interval in the remaining sample locations during subsequent trips (Figure 5 and Table 2). Barometric pressure was removed from all signals and changes in water level were calculated to evaluate the degree of connection between the ocean and inland sample sites. The ratio between the ocean and sample site signal is termed the efficiency, *E*,

232
$$E = \frac{R_a}{F_a}$$
 (1),

Where F_a is the tidal amplitude measured at the forcing boundary (e.g. the coast) and R_a is the tidal amplitude measured at the responding boundary (e.g. the well, borehole, or banana hole). Where efficiency can be measured, we can quantify ocean connection, yet, where efficiency cannot be measured due to a lack in tidal variation, no connection to the ocean can be resolved over tidal timescales.

Modeling perched aquifer conditions

We evaluate the potential for banana holes to form in aquifers perched on exposure zones. The 1-D flow rate which would result in water accumulating on the exposure zone (Q_{in}) must be greater than the flow rate across the zone (Q_{out}) to result in perching. Flow to the aquifer can be estimated as,

$$Q_{in}=RA~(2),$$

where R is the recharge in m/year and A is the catchment area. Flow out of the aquifer can be estimated assuming Darcy's law and constant head,

246
$$Q_{out} = KiA$$
 (3),

where i is the hydraulic gradient and K is the hydraulic conductivity. The hydraulic gradient can be calculated using the thickness of the exposure zone (L), and the height of the water column above the exposure zone (e.g. the aquifer thickness, Δh). Steady state would be achieved for a given set of constants where the Q-ratio is equal to one, and assuming that the area of the exposure zone and the aquifer are the same (e.g. no leakage over the sides), the thickness-permeability pair which would result in a static water level can be calculated by,

253
$$\frac{Q_{in}}{Q_{out}} = \frac{R}{i*K_{steady}} = 1$$
 (4a),

254 and rearranged to

255
$$K_{Steady} = \left(\frac{R}{i}\right)$$
 (4b),

thereby solving for the steady state hydraulic conductivity. Hydraulic conductivity is converted to permeability, k, by,

$$258 K = \frac{k\rho g}{\mu} (5),$$

where ρ is the water density of freshwater (1000 kg m⁻³), μ is the dynamic viscosity of freshwater (8.9x10⁻⁴ pa*s), and g is the gravitational constant. Given that previous studies in the central Bahamas estimate 15-35% (188-438 mm/year) of the annual precipitation (~1250 mm/year) (Wallis *et al.*, 1991; Crump and Gamble, 2004, 2006) is recharged to the aquifer, we can forecast the thickness and permeability pair of an exposure zone required for an aquifer to be perched throughout the year (assuming temporally uniform recharge). Similarly, we can reverse the process by holding aquifer thickness (h) constant and forecasting thickness and permeability pair required for different recharge scenarios.

Dissolution Timescales

Dissolution Estimates from Banana Hole Volumes

We calculated dissolution timescales required to generate banana hole volumes in MIS 5e strandplains for three conceptual models: vadose formation (Whitaker and Smart, 1989), dissolution at water tables (Harris *et al.*, 1995; Gulley *et al.*, 2020, 2015) and prograding strandplains (Mylroie *et al.*, 2016). While some banana holes also occur in MIS9/11 bedrock, we do not estimate timescales for their formation due to the lack of constraints on the timing of bedrock deposition. Using the minimum bounding geometry of each banana hole (2918 in total), we calculated the linear dissolution rates for the P₁₀, P₅₀ and P₉₀ of the calculated banana hole volumes over timeframes ranging from 100 to 125,000 years. The volume of carbonate removal was calculated within the minimum bounding geometry (e.g. m³/km² Figure 6) for all detected MIS 5e banana holes providing the dissolution rate required for a given timeframe.

For models suggesting banana holes formed by vadose processes, we assume that banana holes could have formed at any time after bedrock was deposited (e.g. ~ 125 ka). For the water table cave model, we assume banana holes could have formed at any time during the MIS 5e highstand after bedrock deposition. While we use the full length of the 5e highstand, sufficient sediment accumulation would have to occur on the platform to create the subaerially exposed dunes and strandplains, and thus, only part of the highstand would be suitable for dissolution to occur. As a result, our estimates of dissolution rates represent minimum values. The length of the MIS 5e high stand has been a topic of debate (Hearty and Kindler, 1993; Mylroie and Carew, 1995; Thompson *et al.*, 2011; Kerans *et al.*, 2019b), however, most of these estimates range between 7 and 10 thousand years. For the prograding strandplain model, we assume dissolution would only have occurred in the distal margin of the freshwater lens and stopped as new strandplain accreted. We provide minimum and maximum timeframes for void formation by dividing the length of MIS5e (~7-10 ka) by the number of ridge generations in each

strandplain as observed on the LiDAR DEM. This assumes equal duration for void growth in each new mixing zone over the MIS 5e highstand.

Dissolution Estimates from Excess Calcium Concentrations

292

293

294

295

296

297

298

299

300

301

302

303

304

305

306

307

308

309

310

311

312

313

314

We also calculated dissolution timescales using previously published estimates of dissolution resulting from mixing of fresh and saline waters, and heterogeneous distributions of PCO₂ in ideal systems, which we define as excess Ca²⁺ (Gulley et al., 2015). We used excess Ca²⁺ for the most efficient fresh-seawater ratios to provide maximum rates of dissolution for mixing scenarios (see Gulley et al., 2015, Figure 12). Excess Ca2+ from mixing was reported to range between ~0.1 mmol/l and 0.9 mmol/l while excess Ca²⁺ from heterogeneous distributions of PCO₂ was reported between ~0.9 to 2.25 mmol/l (Gulley et al., 2015). Using these values and an average bedrock porosity of 30%, we estimated the volume of carbonate bedrock removal using the molar volume of aragonite (37.32 cm³ mol⁻¹), and the following assumptions: 1) All waters within the aguifer would reach the assigned Ca²⁺ concentration before being discharged to the ocean 2) Because a freshwater lens at steady state has discharge rates equal to recharge rates (Vacher et al., 1990), the amount of annual carbonate removal from an island of a given catchment area can be estimated using recharge rates 3) While spatial focusing of dissolution will occur within a given platform, the bulk dissolution volumes can be calculated, normalized to area, and applied to an island of any size. We calculated dissolution volumes using recharge values ranging from 100 to 500 mm/year which exceeds the full range of values reported in the central Bahama Islands (188 mm/year: Vacher and Wallis, 1992, and 438 mm/year: Crump and Gamble, 2004). Because our analysis assumes all waters moving through the aquifer would reach the assigned excess Ca²⁺ concentrations before being discharged, the dissolution estimates presented herein represent maximum values.

Results

Banana Hole Size, Distribution, and Abundance

Holocene strandplains cover approximately 15.5 km² of San Salvador Island. All depressions detected in Holocene strandplains were anthropogenic or reflected circular to oval enclosures generated by high angle dune morphologies. Most features falsely identified as collapse features were observed near the airport, Club Med resort, and in high relief Holocene dune ridges on the eastern coast of the island (Figure 4). After verifying detections and eliminating false positives from the data set, not a single banana hole was observed in Holocene strandplains (Figure 9, Figure 10 and Table 3).

MIS 5e strandplains cover approximately 18.5 km² of San Salvador Island (Figure 9 and Figure 10) and contain 2918 banana holes. Most banana holes (2330) were detected in the E1 (or Line Hole) strandplain while a minimum of five banana holes observed in the E5 strandplain (Figure 10 and Table 3). The largest banana hole was 897 m² and the deepest banana hole was just over 6 meters (Figure 10 and Figure 11). Banana hole floors (minimum elevations) were rarely observed below 1-meter elevation and reached a maximum elevation of just below 19 meters RSL in the ridges of E7 (Figure 11A), which is better described as a foredune plain (Hesp, 2011) than a true strandplain. We observed a strong positive correlation between maximum slope angle and banana hole thickness, with the max slope angle reaching about 70 degrees in a 6-meter-deep banana hole (Figure 11B). It is important to recognize that numerous small banana hole features have likely been filtered out of the data set in an attempt to strictly adhere to the field verified parameters (Figure 4).

MIS9/11 strandplains cover approximately 3.9 km² of San Salvador Island (Figure 10). Within MIS9/11 strandplains, 438 banana holes were detected (Figure 10 and Figure 11) with a maximum of 138 observed in the partially flooded P1 strandplain (Figure 4) and a minimum of 11 banana holes observed in the P3 strandplain (Figure 10). Banana hole area reached a

maximum of 647 m², while the maximum depth from the lip to the floor of the banana hole was observed at just over 3.6 meters (Figure 10 and Figure 11). Banana hole floors were rarely observed below 0.5 meters RSL and reached a maximum elevation of up to 11 meters RSL (Figure 11C). The correlation between maximum slope angle and banana hole thickness is nearly identical to that of MIS5 strandplains, yet, the max slope angle only reached 55 degrees in a 3.6-meter-deep banana hole (Figure 11D).

Banana holes in all strandplains fell along dune parallel trends (Figure 12A and B). Higher relief strandplains contained banana holes in restricted linear trends while broader and lower relief strandplains had more variability in banana hole locations (Figure 12). While not currently verified as banana holes, multiple depressions with the same dimensions as banana holes were observed in the valleys of other facies such as tidal flats (Figure 12C). However, we verified the banana hole formed in a dune ridge in the Sandy Point area during the summer of 2017 (Figure 12D).

Connectivity Between Banana Holes and the Aquifer

At the Line Hole strandplain, banana holes partially to completely fill with water during wet seasons (Figure 13A) and are dry during dry seasons (Figure 13B). Neither of the monitored banana holes (BH1 and BH2) showed tidal periodicity in water levels, and thus, efficiency values could not be calculated for either banana hole (Figure 14C and Table 2). However, water levels declined by approximately 5 cm in BH1 and by 7 cm in BH2 over the two-day collection period (Figure 14C). Tidal efficiencies for wells in the Linehole well field varied between 30 and 51 percent and the LH- Deep borehole had an efficiency of 60 percent (Figure 14A and Table 2).

Modeling Perched Aquifer Conditions.

Based on the median exposure zone thickness (0.42 m) and permeability (10^{-16.5} m²), aquifers less than 6 meters in thickness (the maximum relief of observed water filled banana

holes) could become permanently perched on exposure zones given the current recharge estimates (Figure 15A). Holding the aquifer thickness constant (at 3 meters), perched aquifers are possible for all but the most pessimistic recharge scenarios (e.g. less than 5% of precipitation). Given the recharge rates and median exposure thickness, exposure zone permeabilities of about 10^{-15.9} and 10^{-16.3} m² result in perched aquifers (Figure 15B).

Dissolution Rates for Banana Hole Formation.

Estimates from Banana Hole Volumes

Using banana hole volumes ranging between the P₁₀ and P₉₀ of the data, we calculated dissolution rates in MIS 5e strandplains which range between ~2 and 200 m³/km² yr (over 125 ka) for vadose dissolution models (Figure 16). Dissolution rates for voids forming at the water table or mixing zone of the MIS 5e freshwater lens (6-10 ka) range between 40 and 1,000 m³/km² yr (Figure 16). Assuming voids formed in the mixing zone of prograding MIS 5e strandplains, dissolution would occur within each shoreface generated during the MIS 5e high stand. Using the LiDAR data, we estimated MIS 5e strandplains contain between 5 and 18 ridge generations (Figure 4B) thereby subdividing the timeframe for dissolution to occur in each shoreface to between ~ 300 and 2,000 years during the MIS 5e high stand (7-10 ka). As a result, dissolution rates required to form banana hole volumes between the P₁₀ and P₉₀ of the data would range from 200 and 7,000 m³/km² yr (Figure 16).

Estimates from Excess Calcium Concentrations

Mixing of pure freshwaters equilibrated to a PCO₂ of log (-1.0) resulted in excess Ca²⁺ concentrations of 0.1 mmol/l, translating to dissolution rates between 0.48 m³/km² yr and 2.4 m³/km² yr using recharge rates varying from 100 to 500 mm/year respectively. Mixing of fresh and saline end members equilibrated to the same PCO₂ resulted in excess Ca²⁺ concentrations of approximately 0.9 mmol/l, translating to dissolution rates between 4.0 and 20.5 m³/km² per year using the same recharge range (Figure 16). Heterogeneous PCO₂ models overlap with

mixing models at 0.9 mmol/l (Dissolution rate: 4.0 to 20.5 m³/km per year) when PCO₂ increases from log (-2.0) to log (-1.5) along a flow path (Gulley *et al.*, 2015). When PCO₂ Increases from log (-2.0) to log(-1.0) along a flow path, dissolution rates range from 10.1 to 50.4 m³/km² of carbonate per year assuming the same range of recharge values (Figure 16)

Discussion

In the following paragraphs, we discuss the implications of banana hole distributions, their lack of connectivity to the aquifer, and propose a new model for banana hole formation. Our analyses from the LiDAR and hydrologic data suggest that previous interpretations of banana holes as simple vadose pits, water table caves, and syndepositional flank margin caves are at least partially correct. We speculate that surface runoff to discrete recharge points drives dissolution in transient, perched aquifers during sea level low stands. This formation mechanism allows banana holes to form over tens of thousands to hundreds of thousands of years rather than several hundred to a few thousand years as previously suggested.

Size, Distribution and Abundance of Banana holes

Our data support the assessment that banana holes are neither traditional vadose pits nor small collapsed water table caves (Whitaker and Smart, 1989; Harris *et al.*, 1995; Gulley *et al.*, 2015) (Figure 1 and Figure 2). The vadose pit model cannot explain the fully to partially roofed morphologies, and neither model can explain their non-random distributions (Pace and Mylroie, 1993; Harris *et al.*, 1995). In addition, the LiDAR data indicate 61 banana holes with floors at elevations between +8 and +19 meters elevation in dune ridges within the strandplain polygons, which is higher than the frequently reported maximum sea level (+6) occurring during MIS 5e (Figure 11A and Figure 12) and thus, higher than any plausible water table elevation. Consequently, banana holes at high elevations could not have formed at the water table or mixing zone of the MIS 5e freshwater lens. While previous studies have argued that karst features above +6 meters on San Salvador are exclusively pit caves (Harris *et al.*, 1995), the

morphologies of field-verified depressions above +6 meters elevation (Figure 12) are indistinguishable from those of banana holes at lower elevations. For example, the banana hole observed in Sandy Point (Figure 12D) has a width to depth ratio of about 8, an exposed floor area of about 165 m², and an overhung roof along the west-northwest side.

415

416

417

418

419

420

421

422

423

424

425

426

427

428

429

430

431

432

433

434

435

436

437

438

439

Our data also suggest banana holes are unlikely to be forming syndepositionally within prograding strandplains (Mylroie et al., 2016). Under the syndepositional model, voids would be required to reach their full volumes before the mixing zone shifted, and thus, at least some collapse should have occurred in the oldest generations of a strandplain while new generations were still forming (Figure 3). Consequently, banana hole development should be observed in the oldest parts of Holocene strandplains, yet, not a single banana hole is found in the more than 15.5 km² of strandplains (Figure 4B and Figure 10). One could argue that voids exist in the subsurface of Holocene strandplains and have simply not yet collapsed. However, this assumption is only plausible if voids within Holocene strandplains are significantly smaller than MIS 5e banana holes to preclude roof failures. To test this hypothesis, we used estimates of dissolution rate consistent with the prograding strandplain model in MIS 5e and applied them to timescales in Holocene strandplains. In Holocene strandplains, between 6 and 20 (Figure 4B) strand generations have been deposited in 3-5 thousand years, and thus, void formation within each shoreface would have occurred between 150 and 800 years. Using a dissolution rate of 541 m³/km² yr (minimum for prograding strands in MIS5e), 81,150 m³ to 432,800 m³ of carbonate would be dissolved per km² in Holocene bedrock. If we use the average bounding geometry (Figure 6) form MIS5e banana holes (0.00011 km²), void volumes between 8.9 and 48 m³ should have formed in Holocene bedrock. Given that 75% of MIS 5e banana holes are less than 48 m³, and that dissolution rates are likely higher than the value used, we should observe numerous collapsed banana holes in Holocene strandplains if the prograding strandplain model is valid. Further doubt is cast on the existence of Holocene caves because none have been

breached by heavy equipment during road or building developments, and none have been detected in any of the GPR surveys performed in Holocene strand plains (Carney *et al.*, 1993; Markert, 2019). On the contrary, several caves had been breached or geophysically detected in MIS 5e Bedrock during the airport runway extension project (Mylroie, Personal communication, September 23rd, 2021). Conflicts with the syndepositional flank margin caves also arise because banana holes have been found forming within facies other than strandplains (Figure 11C). While not all of these depressions are currently field verified, the banana hole in the Sandy Point is verified in Dune ridge (Figure 12D) and others have been verified with tidal flat facies evident by crenulations in the walls of banana holes in Hard Bargain. Multiple depressions in tidal flats, and lagoons will need to be physically verified (Figure 12C), however, their morphologies on the lidar provide evidence that banana holes are not facies selective karst features.

Evaluating Hydraulic Connectivity Between Banana Holes and the Aquifer

The hydrologic data collected from banana holes suggest that they are disconnected from the modern aquifer. In the Line Hole strandplain, standing water reaches elevations of up to 4 to 5 meters above sea level during the wet seasons (Figure 12A) which is higher than can be explained by a regionally-increased freshwater lens elevation (Figure 13). In addition, strandplains such as P3 contain banana holes which fill with water to 6 plus meters above sea level during wet seasons. Because concurrent water level elevations have not been made in the Line Hole well field and the banana holes, we cannot directly establish that banana holes are disconnected from the aquifer using elevation data alone, even if a 3-5 meter rise in water table elevation is very unlikely. However, the lack of tidal variability in ephemeral banana hole pools cannot be explained by attenuation of the tidal signal between the banana hole and the shoreline (Figure 13). Tidal amplitudes in LH-Deep and the Line hole wells suggest they have efficient ocean connections, yet, BH1 and BH2 show no connection to the ocean (Figure 14). The pressure wave driving water level variations in wells could not travel laterally across the

water table and selectively bypass the banana holes (Figure 5 and Figure 14). Therefore, perching is the only mechanism which can describe water filled banana holes lacking tidal periodicity.

Our data indicate banana holes are perched storage tanks that form preferentially in local topographic lows. Runoff from intense rain events flows downslope and into banana holes where higher heads in the banana holes drive water flow laterally into the surrounding bedrock porosity above the perching surface. Within fully roofed chambers, little evaporation would occur and water level declines would thus reflect slow drainage through the low permeability interval, and discontinuities in the low permeability surface. Where roof collapse has exposed banana holes to the atmosphere, evaporation would account for part of the drainage.

Because banana holes in this study contained about 30-40 cm of water when pressure records were collected (-0.5 meters), we speculate that heads had likely equilibrated with the surrounding matrix and that the 5 to 7 cm decline over the two-day period in BH1 and BH2 reflects drainage across the perching surface (Figure 11C). Correcting for the average daily evaporation (3 mm/day, Crump and Gamble, 2006), and neglecting the 5-7 cm change falling head, we approximate the 1-D hydraulic conductivity of the perching surface to be about 10^{-1.5} m/day, or on the order of 10^{-15.5} m² (Eq. 5). This value is consistent with the upper quartile of permeabilities collected from exposure zones (Figure 5) and is well below permeability values reported for MIS5 bedrock (Breithaupt *et al.*, 2021).

Modeling Perched Aquifer Conditions

Estimates of vertical permeability from pressure records in banana holes are consistent with permeabilities required for perching from our numerical forecasts (Figure 12). Given that the elevation of the land surface around BH1 and BH2 is about +6 to +7 meters above sea level, and the banana hole floors are about 1-2 meters above sea level, the maximum height of the water column would be about 6 meters. Assuming the minimum annual recharge to the perching

surface (188 m/year, Vacher and Wallis 1992) and the permeability estimated from the draining banana holes (10^{-15.5} m²), the thickness of an exposure zone required to perch a 3 meter thick aguifer is about 20 cm (Figure 15A). If the true recharge to the aguifer is closer to the maximum value (35% = 438 mm/year), the perching surface would be required to be about 10 cm thick (Figure 15B). However, the exposure zone thickness required for ephemeral perching is likely overestimated for two reasons: 1) The perching model assumes steady state, which would maintain the water levels throughout the year and 2) surface runoff flowing into banana holes results in locally higher recharge values than diffuse infiltration from rainfall. As a result, an exposure zone could be just a few cm in thickness and still result in temporary perching (Figure 15). Islands like San Salvador contain numerous exposure zones which could act as perching interfaces (Boardman et al., 1995; Mylroie and Carew, 1995; Breithaupt, 2020 Chapter 2). Aquifer perching on exposure zones can describe banana hole formation at high elevations, where the MIS 5e sea levels would not have reached to emplace a freshwater lens. As a result, higher elevation banana holes observed in this study are likely controlled by the position of an underlying exposure zone rather than paleo lenses (Figure 11). While our numerical models for perching conditions are a simplification, they demonstrate that perching can occur above sea level under a number of different recharge, and by extension, climate scenarios well above sea level elevations. Under San Salvador's current climate, both seasonal and permanent freshwater wetlands exist, and have been interpreted to form at least in part due to underlying exposure fabrics which can perch, and isolate them from saline groundwater (Gentry and Davis, 2006; Breithaupt, 2020). In the subsurface, a similar permeability contrast between exposure zones and the host limestone would promote filling and draining cycles during sea level lowstands, thereby dissolving the bedrock and removing solutes multiple times during a wet season.

490

491

492

493

494

495

496

497

498

499

500

501

502

503

504

505

506

507

508

509

510

511

512

A Perched Aguifer Model for Banana Hole Formation

514

515

516

517

518

519

520

521

522

523

524

525

526

527

528

529

530

531

532

533

534

535

536

537

Here we propose our new model for banana holes formation within transient perched aguifers. Shortly after bedrock deposition, surficial calcretes, and paleosols form on the land surface. These low permeability surfaces focus runoff from surrounding dune ridges to local topographic lows (Figure 17 and 18). Waters flowing through high permeability matrix porosity or vadose fast flow routes, such as fractures, root casts and pit caves, in topographic lows would create the initial entry points for water through the exposure zone (Figure 18A and 18B) and accumulation of organic rich soils in shallow surface pits would fuel CO₂ respiration resulting in biogeochemical drilling downward from the surface (Figure 18C and 18D). When dissolution shafts intersect low permeability horizons or exposure zones, downward drilling ceases, and waters are forced laterally into the bedrock porosity above the perching interface (Figure 18E and 18F). Dissolution enlarges the void radially from the injection point during recharge events (Figure 18 C,G,E,I and K). Between rainfall events, water that has equilibrated with carbonate minerals drains through perforations in the exposure zone, emptying the banana hole and the perched aguifer of water and priming the system for dissolution during each subsequent recharge event (Figure 18 D,F,H,J and L). As the void radius increases, the bedrock would become undercut, creating void morphologies which are fully to partially roofed except for the small openings to the surface which deliver waters (Figure 18G). Banana holes which are cut off from supplies of recharge, such as where runoff becomes intercepted by another newly formed banana hole, could support growth of speleothems (Figure 18H and 18J) until ceiling collapse completes the process of banana hole formation (Figure 18K). Assuming banana holes form in perched aquifers would still qualify them as phreatic features, however, these phreatic conditions are decoupled from the main freshwater lens (an epiphreatic condition).

Dissolution Rates: Limitations for Banana Hole Formation.

Banana hole formation in transient perched aquifers is also more consistent with limestone dissolution rates estimated from excess Ca²⁺ concentrations. Phreatic models for banana hole formation have largely assumed that a freshwater lens must be present to dissolve bedrock and form their pre-collapse voids (Mylroie and Carew, 1995; Gulley *et al.*, 2015; Mylroie *et al.*, 2016). Because the position of the freshwater lens tracks with sea levels, opportunities for dissolution to occur at, and above, modern sea levels are limited to short lived sea level high stands (Harris *et al.*, 1995: Florea *et al.*, 2007; Mylroie *et al.*, 2015; Breithaupt *et al.*, 2021). While the biological and geochemical processes proposed above may contribute to cave formation in environments where water tables and/or mixing zones are stable over >10 ka timescales, the dissolution rates required for banana hole formation during the MIS 5e highstand in the Bahamas are orders of magnitude greater than those calculated from the most optimistic mixing and PCO₂ models (Figure 16). Banana hole formation in shifting mixing zones are yet another order of magnitude higher than suggested by mixing and PCO₂ models.

Our proposed model of dissolution within ephemeral perched aquifers results in more reasonable dissolution timescales (Figure 16). Given modern climate conditions, ephermeral perching could occur during the wet seasons for 3-6 months/year, allowing dissolution to occur over more than 30,000-60,000 years since the deposition of MIS 5e bedrock. Although, the exact timeframes for ephemeral perching would be impacted by the climate conditions following the last interglacial. Given the additional timeframe for formation, dissolution rates in the Bahamas more closely align with those published in other settings (Gunn, 1981; Palmer, 1991; Gulley *et al.*, 2014). As a result, there is no need to invoke special circumstances which could result in rapid dissolution to describe the presence of large caves in MIS 5e (and older) bedrock in the Bahamas.

Implications for the Formation of Flank Margin Caves

562

563

564

565

566

567

568

569

570

571

572

573

574

575

576

577

578

579

580

581

582

583

584

585

586

Parallels between flank margin caves and the chambers which collapse to form banana holes have been drawn in the literature on several occasions (Harris et al., 1995; Mylroie and Carew, 1995; Gulley et al., 2015; Mylroie et al., 2016, 2020). Extending our ephemeral perched aquifer model for banana hole formation to flank margin caves would resolve a number of issues for the flank margin cave model. For example, numerous flank margin caves occur at elevations higher than any mid-late Pleistocene sea levels (Mylroie et al., 2020). A prime example is "Big Cave" in Mt Alvernia in Cat Island (Mylroie and Mylroie, 2013), which is about 63 meters above modern sea level and has been speculated to have formed on a paleosol in a perched aquifer system (Mylroie and Mylroie 2013). Caves between +8 meters and +24 meters RSL, however, have been interpreted to from within one or more freshwater lenses, and speculated to have been uplifted to their present position rendering their utility as sea level indicators suspect (Mylroie et al., 2020). Uplift could be driven by denudation and removal of surficial deposits, thereby resulting in isostatic rebound while simultaneously accounting for the reported lack in subtidal facies older than MIS 5e across the Bahamas (Mylroie et al., 2020). However, a paradigm shift in the archipelago-wide tectonic regime is not necessary to describe caves at higher elevations if they formed in perched aquifers. In addition, the large volumes of some flank margin caves, which have been attributed to multiple lens emplacements during more than one sea level highstand (Mylroie et al., 2020), would not be required. If caves form in an epiphreatic aquifer perched above sea levels, they could be the result of hundreds of thousands of years of episodic growth rather than forming within one or more freshwater lenses over tens of thousands of years or less (Figure 16). Evidence for the formation of caves in perched aguifers is strong in San Salvador, and in several cases paleosols and calcretes have been observed constraining the vertical position of flank margin caves across the Bahamas (See Mylroie et al., 2020; Figure 6)

The development of the perched aquifer model is not to suggest that freshwater lenses do not contribute to dissolution and cave formation. The distinct expression of freshwater lenses can be observed in the Danian karst where the stable position of paleo-lenses on the order of millions of years has resulted in spectacular vug and cave networks extending over 10 kilometers (e.g. Baceta *et al.*, 2001, 2007). However, future work should address the hydraulic properties of perching zones directly beneath cave chambers to assess the potential for formation within perched aquifer systems, particularly in settings where formation timescales are short.

6.0 Conclusion

587

588

589

590

591

592

593

594

595

596

597

598

599

600

601

602

603

604

605

606

607

608

609

610

611

Banana holes are dissolutional voids which form within ephemeral aquifers perched in the vadose zone. Geospatial and hydrologic data indicate banana holes form along dune parallel trends when runoff focused to catchments is delivered to the subsurface through fast flow routes and becomes forced laterally into the bedrock above exposure zones. Episodic undercutting of the bedrock during wet seasons enlarges voids below the land surface creating fully roofed cave morphologies. Enlargement eventually leads to collapse and exposure to the atmosphere, thereby resulting in the partially roofed pits observed in the Bahamas today. Past models have suggested that banana holes could only form within paleo-freshwater lenses during sea level high stands. However, our data demonstrate that phreatic diagenesis and the formation of dissolutional voids can occur in perched aguifers during sea level low stands. Because waters can become perched on exposure zones, dissolution rates calculated using banana hole volumes are more consistent with dissolution rates derived from thermodynamic and kinematic methods. As a result, no accelerated dissolution mechanism is needed to describe their occurrence. We suggest banana holes, and flank margin caves alike represent hundreds of thousands of years of episodic dissolution within perched aquifers rather than dissolution during one or more freshwater lens emplacements.

612	Acknowledgments
613	Funding for this project came from ExxonMobil Upstream Research Company and NSF
614	EARGrant #1743383. We thank Andrea Nolting, Antonio Buono, Brian Kelly, Michelle Dafov,
615	Glenn Thompson, and John Mylroie for several insightful and thought-provoking conversations.
616	We would also like to thank Troy Dexter, Sledge Simmons, Mark Constant, and other staff at the
617	Gerace Research Center for logistical support. All research was conducted under a permit
618	issued by the Bahamas Environment, Science and Technology (BEST) Commission. We thank
619	Randolph Simpson, Daniel Anderson, Bradford Mack, Gregory Russo, Lauren Mancewicz,
620	Captain Bruce Niro, and Nigel Spaxman for field and technical support. Lastly, we acknowledge
621	critical moral support derived from John Watling, Barritt, Wendy's snack bar, and Club Med
622	resort.
623	Conflict of interest
624	None.
625	Data availability statement
626	The datasets used and/or analyzed during the current study are available from the
627	corresponding author on request.
628	
629	
630	
631	References
632 633 634	Baceta, J.I., Wright, V.P. & Pujalte, V. (2001) Palaeo-mixing zone karst features from Palaeocene carbonates of north Spain: criteria for recognizing a potentially widespread but rarely documented diagenetic system. Sedimentary Geology, 139(3–4), 205–216.

- Baceta, J.I., Wright, V.P., Beavington-Penney, S.J. & Pujalte, V. (2007) Palaeohydrogeological
- control of palaeokarst macro-porosity genesis during a major sea-level lowstand: Danian of the
- 637 Urbasa–Andia plateau, Navarra, North Spain. Sedimentary Geology, 199(3–4), 141–169.
- 638 https://doi.org/10.1016/j.sedgeo.2007.01.024
- Boardman, M.R., McCartney, R.F., Eaton, M.R., (1995) Bahamian Paleosols: Origin, relation to
- paleoclimate, and stratigraphic significance. Terrestrial and shallow marine geology of the
- Bahamas and Bermuda, H. Allen Curran, Brian White
- Bottrell, S.H., Carew, J.L., Mylroie, J.E. (1993) Inorganic and bacteriogenic origin for sulfate
- crusts in flank margin cave, San Salvador Island, Bahamas. In: White, B., (Ed.) Proceedings of
- the 6th Symposium on the Geology of the Bahamas Bahamian Field Station, San Salvador, pp.
- 645 17-21.
- Breithaupt, C.I., 2020. Porosity and permeability extremes in an eogenetic carbonate platform:
- 647 mechanisms for formation and implications for fluid flow. Ph.D. dissertation. University of South
- 648 Florida, p 1-202
- Breithaupt, C. I., J. D. Gulley, P. J. Moore, S. M. Fullmer, C. Kerans, and J. Z. Mejia, 2021,
- Flank margin caves can connect to regionally extensive touching vug networks before burial:
- 651 Implications for cave formation and fluid flow: Earth surface processes and landforms, v. 46, no.
- 652 8, p. 1458–1481, doi:10.1002/esp.5114
- 653 Carew, J.L., Mylroie, J.E., (1991) Some pitfalls in paleosol interpretation in carbonate
- sequences. Carbonates and Evaporites 6, 69–74. https://doi.org/10.1007/BF03175383
- 655 Carney, C., Stoyka, G.S., Boardman, M.R., and Kim, N., (1993) Depositional History and
- Diagenesis of a Holocene Strand Plain, Sandy Hook, San Salvador, Bahamas. In: White, B.,
- 657 (Ed.) Proceedings of the 6th Symposium on the Geology of The Bahamas. San Salvador:
- 658 Gerace Research Center, College of the Bahamas, pp. 35-46
- 659 Cooper, K.J., Whitaker, F.F., Anesio, A.M., Naish, M., Reynolds, D.M., Evans, E.L., (2016)
- 660 Dissolved organic carbon transformations and microbial community response to variations in
- recharge waters in a shallow carbonate aguifer. Biogeochemistry 129, 215–234.
- 662 https://doi.org/10.1007/s10533-016-0226-4
- 663 Crump, M., Gamble, D., (2006) Spatial Variability of Precipitation on Sn Salvador, Bahamas
- 2001-2003, in: Laurence Davis, D.G. (Ed.), 12th Symposium of the Geology of the Bahamas
- and Other Carboate Regions. Gerace Research Center, San Salvador Island, Bahamas, pp.
- 666 52-60.
- 667 Crump, M., Gamble, D., (2004) Climate-derived water budget and synoptic-scale precipitation
- pattern analysis., in: College of the Bahamas (Ed.) Proceedings of the 11th Symposium on the
- Geology of the Bahamas and other Carbonate Regions 2002. San Salvador: Gerace Research
- 670 Center, College of the Bahmas, pp. 127–134.
- 671 Davis, R.L. & Johnson, C.R. (1989) Karst hydrology of San Salvador. In: Mylroie, J.E. (Ed.)
- 672 Proceedings of the 4th Symposium on the Geology of the Bahamas 1988. San Salvador:
- 673 Gerace Research Centre, College of the Bahamas, pp. 118–135.

- Florea, L.J., Vacher, H.L., Donahue, B. & Naar, D. (2007) Quaternary cave levels in peninsular
- Florida. Quaternary Science Reviews, 26, 1344–1361.
- 676 https://doi.org/10.1016/j.quascirev.2007.02.011
- 677 Gentry, CL and RL Davis (2006) The Geomorphological and Hydrological Controls of Fresh
- Water Wetlands on San Salvador Island, Bahamas, in: Davis, L., Gamble, G., (Ed.) Proceedings
- of the 12th Symposium on the Geology of The Bahamas, p. 61-68.
- 680 Godefroid, F., Kindler, P., Chiaradia, M. & Fischer, G. (2019) The Misery Point cliff, Mayaguana
- Island, SE Bahamas: a unique record of sealevel highstands since the early Pleistocene. Swiss
- 682 Journal of Geosciences, 12, 287–305. https://doi.org/10.1007/s00015-018-0323-6
- 683 Gulley, J.D., Breecker, D., Covington, M., Cooperdock, S., Banner, J., Moore, P.J., Noronha, A.,
- Breithaupt, C., Martin, J.B., Jenson, J., (2020) Tidal pumping and biogeochemical processes:
- 685 Dissolution within the tidal capillary fringe of eogenetic coastal carbonates. Earth Surfurce
- 686 Processes and Landforms 45(11), 2675-2688. https://doi.org/10.1002/esp.4922
- 687 Gulley, J.D., Martin, J.B., Moore, P.J., Brown, A., Spellman, P.D. & Ezell, J. (2015)
- Heterogeneous distributions of CO2 may be more important for dissolution and karstification in
- coastal eogenetic limestone than mixing dissolution. Earth Surface Processes and Landforms,
- 690 40(8), 1057–1071. https://doi.org/10.1002/esp.3705
- 691 Gulley, J.D., Martin, J.B. & Moore, P.J. (2014) Vadose CO2 gas drives dissolution at water
- tables in eogenetic karst aquifers more than mixing dissolution. Earth Surface Processes and
- 693 Landforms, 39(13), 1833–1846. https://doi.org/10.1002/esp.3571
- 694 Gulley, J.D., Martin, J.B., Moore, P.J. & Murphy, J. (2013) Formation of phreatic caves in an
- 695 eogenetic karst aquifer by CO2 enrichment at lower water tables and subsequent flooding by
- sea level rise. Earth Surface Processes and Landforms, 38, 1210–1224. https://doi.org/10.
- 697 1002/esp.3358
- 698 Gunn, J., (1981) Prediction of limestone solution rates from rainfall and runoff data: Some
- comments. Earth Surface Processes and Landforms, 6(6), 595–597.
- 700 https://doi.org/10.1002/esp.3290060609
- Harris, J.G., Mylroie, J.E. & Carew, J.L. (1995) Banana holes: unique karst features of the
- 702 Bahamas. Carbonates and Evaporites, 10, 215–224. https://doi.org/10.1007/BF03175406
- Hearty, P.J. & Kindler, P. (1993) New perspectives on Bahamian geology San-Salvador Island,
- Bahamas. Journal of Coastal Research, 9, 577–594.
- Hesp, P., (2011). Dune Coasts, Treatise on Estuarine and Coastal Science, (3), 193-221.
- 706 Elsevier Inc. https://doi.org/10.1016/B978-0-12-374711-2.00310-7
- 707 Infante, L. (2012) The origin of banana holes on San Salvador Island, The Bahamas, Master's
- 708 Thesis. Mississippi State University: Starkville, MS.
- Jasiewicz, J., Stepinski, T.F., 2013. Geomorphons-a pattern recognition approach to
- 710 classification and mapping of landforms. Geomorphology 182, 147–156.
- 711 https://doi.org/10.1016/j.geomorph.2012.11.005

- Kerans, C., Nolting, A., Fullmer, S., Moore, P.J., Gulley, J.D., Hsia, S.et al. (2019) Lidar-guided
- stratigraphic model of Pleistocene strata, San Salvador Island, Bahamas: sea-level
- reconstructions, sedimentologic models, and carbonate platform development. In: Earth
- Processes. San Francisco: American Geological Union (Lecture) PP41C 1567.
- Kerans, C., Zahm, C., Bachtel, S.L., Hearty, P., Cheng, H., (2019b) Anatomy of a late
- 717 Quaternary carbonate island: Constraints on timing and magnitude of sea-level fluctuations,
- 718 West Caicos, Turks and Caicos Islands, BWI. Quaternary Science Reviews, 205, 193–223.
- 719 https://doi.org/10.1016/j.quascirev.2018.12.010
- Kunze, G. & Sauter, A. (1989) In: Mylroie, J. (Ed.) Geoelectrical survey of the Columbus
- Landings I Region of San Salvador Bahamas 1989. San Salvador: Gerace Research Centre,
- 722 College of the Bahamas, pp. 191–202.
- Markert, Kaleb Robert, "Depositional Analysis of a Holocene Carbonate Strand Plain Using High
- 724 Resolution GPR, Sediment Analysis, and C-14 Dating" (2019). Theses and Dissertations. 7751.
- 725 https://scholarsarchive.byu.edu/etd/7751
- 726 Moore, P., Seale, D. & Mylroie, J. (2004) Pit cave morphologies in eolianites: variability in
- primary structure control. In: Martin, R. & Panuska, B. (Eds.) Proceedings of the 11th
- 728 Symposium on the Geology of the Bahamas and Other Carbonate Regions. San Salvador,
- 729 Bahamas: Gerace Research Centre.
- 730 Mullins, H.T. & Lynts, G.W. (1977) Origin of the northwestern Bahama Platform: review and
- reinterpretation. Geological Society of America Bulletin, 88, 1447–1461.
- 732 Mylroie, J.E., Lace, M., Albury, N. & Mylroie, J. (2020) Flank margin caves and the position of
- mid- to late Pleistocene sea level in the Bahamas. Journal of Coastal Research, 36(2), 249.
- 734 https://doi.org/10.2112/ JCOASTRES-D-18-00174.1
- 735 Mylroie, J.E., Ho, H.C., Infante, L.R., Kambesis, P.N. & Leist, J.W. (2016) Banana holes as
- 736 syndepositional flank margin caves within an advancing strandplain and their prediction using
- 737 fuzzy-based spatial modeling. In: Proceedings of the 16th Symposium on the Geology of the
- 738 Bahamas and other Carbonate Regions. Gerace Research Centre: San Salvador, Bahamas,
- 739 pp. 222–236.
- Mylroie, J.E. & Carew, J.L. (2008) Field guide to the geology and karst geomorphology of San
- 741 Salvador island. Gerace Research Center, 88, 1–90.
- Mylroie, J. & Carew, J. (1995) Geology and karst geomorphology of San Salvador Island,
- 743 Bahamas. Carbonates and Evaporates, 10(2), 193–206. https://doi.org/10.1007/BF03175404
- Pace, M., Mylroie, J., (1993) Investigation and Review of Dissolution Features on San Salvador
- 745 Island, Bahamas, in: Carew, J.L. (Ed.) Gerace Research Center, San Salvador Island,
- 746 Bahamas, pp. 109–123.
- Palmer, A.N. (1991) Origin and morphology of limestone caves. Geological Society of America
- 748 Bulletin, 103, 1–21. https://doi.org/10.1130/0016-7606(1991)103<0001:OAMOLC>2.3.CO;2
- Plummer, L.N. (1975) Mixing of sea water with calcium carbonate groundwater. Geological
- 750 Society of America Memoirs, 142, 219–236.

- Rossinsky, J., and H. R. Wanless, (1992) Topographic and vegetative controls on calcrete
- formation, Turks and Caicos islands, British West Indies: Journal of sedimentary petrology, v.
- 753 62, no. 1, p. 84–98, doi:10.1306/D4267898-2B26-11D7-8648000102C1865D.
- Smart, P.L., Whitaker, F.F., (1989) Controls on the Rate and Distribution of Carbonate Bedrock
- Dissolution in the Bahamas, in: Proceedings of the Fourth Symposium on the Geology of the
- 756 Bahamas. pp. 313–321.
- 757 Tarbox, DL. (1987) Occurrence and development of water resources in the Bahama Islands,
- Proceedings of the 3rd Symposium on the Geology of the Bahamas Bahamian Field Station,
- 759 San Salvador, p. 139-144.
- Thompson, W. G., H. A. Curran, M. A. Wilson, and B. White, (2011) Sea-level oscillations during
- the last interglacial highstand recorded by Bahamas corals: Nature geoscience, v. 4, no. 10, p.
- 762 684–687, doi:10.1038/NGEO1253.
- USACE (2004) Water Resources Assessment of the Bahamas. Mobil District and Topographic
- 764 Engineering Center.
- 765 Vacher, H.L. (1988) Dupuit-Ghyben-Herzberg analysis of strip-island lenses. GSA Bulletin, 100,
- 766 p. 580–591.
- Vacher, H.L., Bengtsson, T.O. & Plummer, L.N. (1990) Hydrology of meteoric diagenesis:
- Residence time of meteoric ground water in island fresh-water lenses with application to
- aragonite-calcite stabilization rate in Bermuda. Bulletin of the Geological Society of America,
- 770 102, p. 223–232. https://doi.org/10.1130/0016-7606(1990)102<0223: HOMDRT>2.3.CO;2
- 771 Vacher, H.L. & Wallis, T.N. (1992) Comparative hydrogeology of fresh-water lenses of Bermuda
- and Great Exuma Island, Bahamas. Groundwater, 30, p. 15–20.
- Wallis, T.N., Vacher, H.L., Stewart, M.T., (1991) Hydrogeology of freshwater lens beneath a
- Holocene strandplain, Great Exuma, Bahamas. Journal of Hydrology (Amsterdam), 125, p. 93–
- 775 109, doi:/10.1016/0022-1694(91)90085-V
- 776 Whitaker, F.F. and Smart, P.L., (1989) controls on the rate and distribution of carbonate bedrock
- dissolution in the Bahamas. Hydrology, 84, p. 333–343.
- 778 Whitaker, F. F., and Smart, P.L., (2007) Geochemistry of meteoric diagenesis in carbonate
- islands of the northern Bahamas: 1. Evidence from field studies: Hydrological processes, v. 21,
- 780 no. 7, p. 949–966, doi:10.1002/hyp.6532.
- Wilson, W.L., Beck, B.F., (1992) Hydrogeologic Factors Affecting New Sinkhole Development in
- 782 the Orlando Area, Florida. Ground Water 30, 918–930. https://doi.org/10.1111/j.1745-
- 783 6584.1992.tb01575.x
- Wright, V. P., (1994) Paleosols in shallow marine carbonate sequences: Earth-science reviews,
- 785 v. 35, no. 4, p. 367–395, doi:10.1016/0012-8252(94)90002-7.

Table 1: Strand Plain Name, Age, And Location

Polygon	Age	Location
(Name)	(Name)	(Name)
H1	Holocene	Barkers Point
H2	Holocene	Bonefish Bay
H3	Holocene	Cockburntown
H4	Holocene	Fernandez bay
H5	Holocene	Snow bay
H6	Holocene	sandy hooke
H7	Holocene	N. crab cay
H8	Holocene	S. Crab cay
H9	Holocene	Halls landing
H10	Holocene	Grotto beach
H11	Holocene	Greens Harbor
H12	Holocene	Hanna bay
H13	Holocene	Grahams Harbor
E1	MIS 5e	Linehole
E2	MIS 5e	Airport
E3	MIS 5e	Sugar Loaf
E4	MIS 5e	Fernandez bay
E5	MIS 5e	Grotto beach
E6	MIS 5e	Frenchbay E
E7	MIS 5e	Hard Bargain
E8	MIS 5e	N hard bargain
E9	MIS 5e	Six Pack
E10	MIS 5e	Granny Lake
P1	MIS 9/11	Great Lake
P2	MIS 9/11	Duck pond
P3	MiS 9/11	Old Place

Table 2: Location of borehole, wells, and banana holes sampled for tidal periodicity

Location (Name)	Relative age (Well Bottom)	X (Distance)	Collection Dates (MM/DD/YY)	Latitude (degrees)	Longitude (degrees)
BH1	Paleosol	239	7/26/2018-7/27/2018	24.1144	-74.4876
BH2	Paleosol	523	7/26/2018-7/27/2018	24.1123	-74.4895
LH1	MIS 5	180	07/24/25-07/27/15	24.1149	-74.4878
LH4	MIS 5	302	07/24/25-07/27/15	24.1138	-74.4882
LH8	MIS 5	424	07/24/25-07/27/15	24.1130	-74.4888
LH13	MIS 5	544	07/24/25-07/27/15	24.1119	-74.4893
LH-Deep	Pre-MIS 5	154	7/26/2018-7/27/2018	24.1151	-74.4873

Table 3: Banana Hole Density By Strand Plain

Polygon Polygon area polygon area # banana holes Density						
(Name)	(m ²)	(km²)	(#)	(#/km²)		
H1	2833635	2.8	0	0		
H2	1053974	1.1	0	0		
H3	413996	0.4	0	0		
H4	796164	0.8	0	0		
H5	371710	0.4	0	0		
H6	380122	0.4	0	0		
H7	1754198	1.8	0	0		
H8	2070436	2.1	0	0		
H9	1235396	1.2	0	0		
H10	947804	0.9	0	0		
H11	1305646	1.3	0	0		
H12	1782162	1.8	0	0		
H13	579276	0.6	0	0		
E1	4706735	4.7	2330	495		
E2	2824996	2.8	157	56		
E3	1262677	1.3	60	48		
E4	1231304	1.2	74	60		
E5	362844	0.4	5	14		
E6	2145915	2.1	73	34		
E7	4997510	5.0	114	23		
E8	480609	0.5	6	12		
E9	246443	0.2	84	341		
E10	285546	0.3	15	53		
P1	2738377	2.7	377	138		
P2	417406	0.4	11	6868		
P3	740000	0.74	50	68		

Figure 1: Conceptual model for banana hole formation in the vadose zone. (A) An undulating bedrock surface collects organic debris which breaks down to form organic rich soils and focuses runoff to topographic lows. (B) Microbial oxidation elevates soil CO2 which acidifies waters percolating though the soil zone and deepens initial surface depressions. (C) Continued accumulation of soils promotes the colonization of depressions with vegetation which increase soil CO2 though root respiration. (D) Denudation, and rock fatigue introduce fracturing into banana hole walls which later collapse as the pit continues to deepen. (E) Large trees with extensive root systems brecciate the host rock as they drill to the water table. (F) Substantial brecciation and rooting leads to soil loss. Illustrations are modified from Whitaker and Smart (1989).

Figure 2: Conceptual models for phreatic origin of banana holes. (A1) Mixing of meteoric and phreatic waters or (A2) diffusion of vadose CO2 gas to the water table initiates the growth of dissolution voids at the water table. Void growth continues in the same locations because fast flow routes cause (B1) repeated mixing or (B2) repeated elevation of CO2 when organic matter delivered to the water table is oxidized. Individual voids grow together through increasing of (C1) the mixing radius or (C2) increasing durations of CO2 injection to the water table. (D) Dropping sea level places caves in the vadose zone and halts cave enlargement. In the vadose zone humid cave chambers promote the growth of speleothems. (E) Loss of buoyant support, denudation, and rock fatigue induce varying degrees of collapse, forming banana holes. Illustrations are based on concepts described in Harris et. al., (1995) and Gulley et. al., (2015).

 Figure 3: Conceptual model for banana holes as syndepositional flank margin caves forming within an advancing strand plain. (A) A freshwater lens invades newly deposited land placing a mixing zone near the shoreface. (B) Pausing of the mixing zone at the shoreface drives dissolution, thereby creating a small flank margin cave. (C) Deposition of the next strandplain generation results in the mixing zone shifting, and thus, dissolution is halted in the original cave chamber and is initiated at the new shoreface. (D) The new mixing zone results in another immature flank margin cave. Continued progradation of the strand plain and episodic shifting of the mixing zone (E) creates multiple cave chambers advancing toward the shoreline. (F) Older generations of these caves may collapse as new caves are still forming. (G) Falling sea levels place cave chambers in the vadose zone where they accumulate speleothems before (H) some collape to form banana holes. Illustrations are based on concepts described in Mylroie et. al., (2016).

Figure 4: (A) Satellite photo from digital globe modified from Kerans et. al., 2018 (B) airborne LiDAR derived digital elevation model collected and processed by NCALM and (C) geologic map of San Salvador Island Bahamas modified from Kerans et. al (2018). Our study focuses on Holocene, MIS 5e and MIS 9/11 strand plains.

Figure 5: (A) Exposure zone thicknesses and (B) permeabilities from the Sandy Point region of San Salvador Island Bahamas. Diagram illustrating compositional elements commonly found in exposure zones. Exposure Zone Data From: Breithaupt 2020., Chapter 2 Figure 6: Field validated data from 71 banana holes near Line Hole well field, Jake Jones road, Hard Bargain, and Victoria Hill. (A) Banana hole areas, (B) length to width ratio, (C) and elevation ranges used to constrain LiDAR detections to banana hole morphologies. Field validated data from Infante et. al., (2012).Figure 7: Location of sample sites at the Line Hole well field on the LIDAR derived digital elevation model. Hot colors represent higher elevations while cool colors represent lower elevations. We collected pressure records in each of the labeled locations over several trips. Several banana holes (similar to those labeled BH1 and BH2) are observed surrounding the sample locations. The floor elevations of banana holes are about 1-2 meters RSL (e.g. the color bar). Figure 8: Illustration of parameters collected from banana holes and limitations of the LiDAR guided analysis of banana hole distributions. The maximum scan angle of the lidar is 60 degrees, however steeper slopes can be calculated when opposite side of depressions are intersected by the laser. The minimum elevation represents the floor of the banana hole, the maximum elevation represents the lip, and the elevation range represents the total thickness. The total thickness will overestimate the dissolutional cave height, which is the distance between the floor and overhang. The minimum bounding length (MBL) and width are used to calculate minimum bounding area (MBA) of the banana hole. Banana hole areas correspond to the exposed floor area while portions under overhangs cannot be quantified with LiDAR data. Figure 9: (A) Comparison between detection of depressions in low relief strand plains at E1 and H1 and (B) high relief strand plains at H7 and H11. A high density of banana holes were observed in (C) Pleistocene strand plains while all detections of depressions in (D) Holocene strand plains were determined to be false positives. Most false positives were due to anthropogenic enclosures, such as pools, pits and rubble piles, however, some natural dune morphology resulted in steep walled circular pits which were removed manually given their similarity to the filtering scheme. Figure 10: Summary of (A) area, (B) elevation range (thickness) and (C) densities of banana holes by strand plain. Yellow polygons represent Holocene strandplains, orange represent MIS 5e strandplains and gray represent MIS 9/11 strandplains. Note the large number of outliers in E1 which has the highest

karst density of all strand plains on San Salvador island. All box plots use a different sample population

based on their strand location. BH = Banana Hole.

876

877

878

879

880

881

882

883

884

885 886

887

888

889

890

891

892

893

894

895

896

897

898

899

900

901

902

903

904

905

906

907

908

909

910

911

Figure 11: (A) Elevation of MIS 5e banana hole floors vs area and (B) banana hole elevation range vs. maximum slope angle. (C) Elevation of MIS9/11 banana hole floors vs area and (D) banana hole elevation range vs. maximum slope angle. See Figure 8 for key to measurement types. Banana hole floors are observed above 6 meters elevation in MIS 5e strand plains and thus could not have formed at past water tables. We observe a large number of banana hole floors which are between 1 and 6 meters RSL but very few below 1 meter suggesting a possible horizon or contact controlling banana hole elevations. High slope angles in banana holes likely represent more recently collapsed pits while shallower angles represent banana holes which have undergone denudation thereby reducing their slope angles as pits partially fill in. The impact of denudation can be observed between MIS 5e and MIS 9/11 banana given the general shallowing of banana holes with time. The post-collapse down wasting has likely removed many banana holes from the MIS9/11 surface or made them undetectable due to infilling. Thus, the density of MIS 9/11 banana holes is likely underestimated.

Figure 12: (A) Examples of banana holes observed in the E2 Strandplain (B) the E7 foredune plain, (C) tidal flat facies, and (D) dune facies. The elevations of several banana hole floors (white numbers) are above the +6 meter sea level elevation reported for the MIS 5e highstand and thus could not have formed in the MIS 5e freshwater lens.

Figure 13: Satellite images of banana holes in the Line Hole strand plain during (A) wet and (B) dry seasons. During wet seasons banana holes become almost entirely filled with rainwater while they are usually empty during the dry seasons. Elevations near the tops of banana holes are between 4 and 5 meters above sea level, and thus, water levels must be elevated above the rest of the water table.

Figure 14: Tidal records in the Line hole well field (A), LH-Deep (B), and two banana holes (C). Strong tidal periodicity is observed in the Line Hole wells and LH-Deep, yet, no tidal signal is observed in BH1 or BH2. We suggest the lack in tidal periodicity indicates the banana holes are disconnected from the underlying aquifer. The decrease in water level in BH1 and BH2 indicate slow drainage of water from the banana hole across the perching interface.

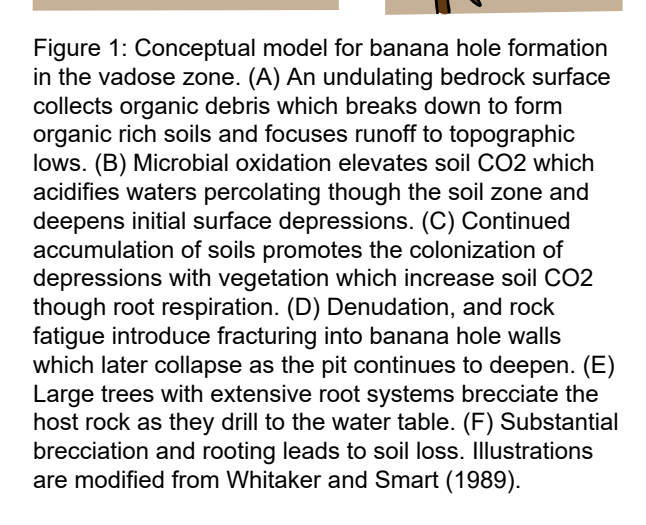
Figure 15: One dimensional perched aquifer model assuming no lateral flow and constant head. (A) Estimates for exposure surface thickness and permeabilities required to maintain perched aquifers between 1 and 25 meters assuming a constant recharge of 188 mm/year or 15% of annual precipitation. (B) Estimates of exposure thickness and permeability required to maintain an aquifer 3 meters in thickness for varying recharge magnitudes. We include the 1st quartile, median and 3rd quartile values for exposure surface thickness and permeabilities as measured from core plugs and core descriptions (Breithaupt 2020, Chapter 2). Recharge between 15 and 35% of annual precipitation have been estimated for islands such as San Salvador (Crump and Gamble, 2006) and Exuma (Vacher and Wallis 1991) and are used to bracket the likely magnitudes.

Figure 16: (A) Dissolution rates estimated given different time-frames for banana hole and flank margin cave formation on San Salvador Island. The dissolution rate is calculated for the P90, P50, and P10 of 2918 banana hole volumes in MIS 5e bedrock. We also estimate dissolution rates for some of the largest flank margin caves (Altar, Majors and Lighthouse) in both MIS 5e and MIS9/11 bedrock. Dissolution rates required to create banana holes in a prograding strand plain are highlighted in blue, within the freshwater lens during MIS 5e are highlighted in green, and in perched aquifers are highlighted in yellow. The gray shaded area represents dissolution rates for Altar, Major's and Lighthouse caves, while the arrow shows the cumulative time frame freshwater lenses could have occupied MIS 9/11 bedrock and the corresponding dissolution rate required to create Majors and Lighthouse caves. (B) Dissolution rates derived from excess Ca2+ in water samples on San Salvador plotted against recharge. Excess Ca2+ values are from published data in the Sandy Point and Line hole well fields (Gulley et al., 2015) and recharge rates are bracketed from previously published values (e.g. Vacher and Wallis 1991 and Crump and Gamble (2006)). Dissolution rates required to create banana holes in 300 to 2000 years (progradational FMC model) are about 2 orders of magnitude greater than values calculated from both heterogeneous PCO2 and mixing models. Banana holes forming between 2 and 10 thousand years require dissolution rates an order of magnitude greater than those from heterogeneous PCO2 and mixing models. Only the perched aquifer model yields dissolution rates consistent with models calibrated to measured excess Ca2+ in San Salvador.

Figure 17: Map view conceptualization of topographic controls on banana hole formation. (A) Strand plains are deposited on the platform. Due to high matrix porosity and lack of surface induration, meteoric waters rapidly infiltrate though the matrix porosity, and little runoff is focused to topographic lows. (B) Calcretes and paleosols begin developing immediately after bedrock deposition as cementation creates indurated surfaces. Over longer durations of exposure, thick calcretes and paleosols form. Indurated crusts on the land surface allow recharge to flow to catchments between ridges, where heterogeneities deliver aragonite and calcite undersaturated waters to the subsurface driving void formation. (C) Voids initially are completely enclosed beneath the land surface, forming large single chambered caves before collapse. Continued denudation and weathering result in more collapse over time and once open to the atmosphere banana holes accumulate soils.

Figure 18: Perched aquifer model for banana hole formation in San Salvador Island, Bahamas. (A) Bedrock deposited during MIS 5e is exposed on the platform entering the low stand. (B) Initial formation of heterogeneities in the topographic lows are driven by fracturing and roots boring through bedrock to ephemerally perched water tables. (C) Regular exposure to meteoric recharge causes surficial calcretes and paleosols to form on the land surface, driving runoff to topographic lows where infiltration occurs through high permeability matrix porosity, fractures, and root casts. (D) Preferred pathways for recharge are dissolutionally enlarged by descending waters, and progressively deepen with each rainfall event. until intersecting a permeability interface. (E) As waters intersect the low permeability surface, they are forced laterally along the interface thereby under-cutting bedrock and resulting in thin lateral chambers above the permeability interface. (F) During dry seasons, waters slowly drain across the surface and dissolution ceases, and thin chambers become air-filled. (G) Repeated filling and draining cycles result in thin, laterally extensive chambers, which begin to collapse due to wide spans thereby vertically

migrating the void space. Collapse blocks may become encased in organic rich soils which act to increase CO2 concentrations and more efficiently dissolve blocks during filling and draining cycles. H) Air filled chambers may grow speleothems on their roof and walls. (I) Continued collapse begins to expose voids to the atmosphere allowing larger vegetation to grow in organic rich soils. (J) Pit caves which had been forming simultaneously, yet at a slower rate due to lower runoff volumes, begin to reach the low permeability interface and enlarge voids. (K) Modern day banana holes have overhung to collapsed roofs, contain soil mats in their floors, and of course, often contain banana trees. (L) During modern wet seasons, banana holes become filled with waters perched on permeability boundaries and are disconnected from the underlying aquifer. Permeability boundaries may be composed of exposure zones, facies boundaries, or mineralogical contacts.



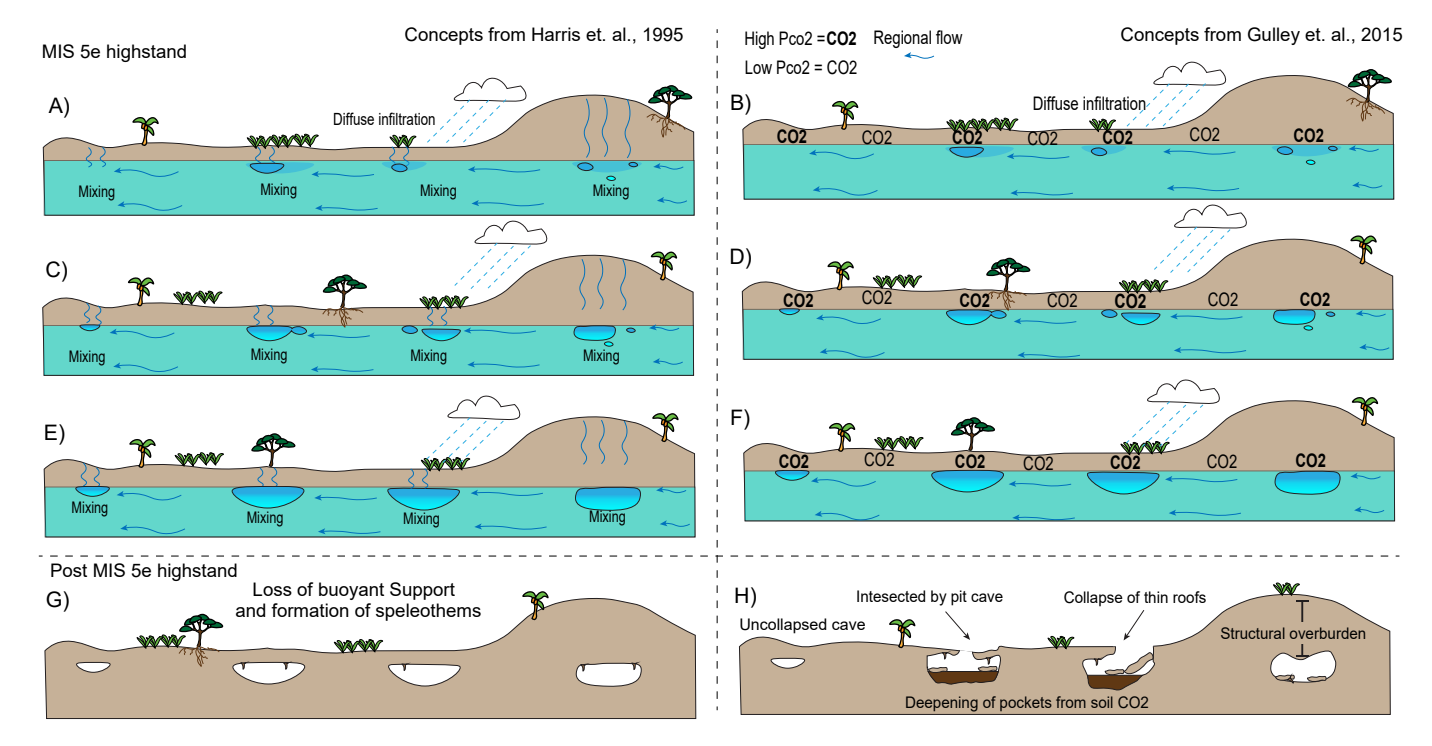


Figure 2: Conceptual models for phreatic origin of banana holes. (A) Mixing of meteoric and phreatic waters or (B) diffusion of vadose CO2 gas to the water table initiates the growth of dissolution voids at the water table. Void growth continues in the same locations because fast flow routes cause (C) repeated mixing or (D) repeated elevation of CO2 when organic matter delivered to the water table is oxidized. Individual voids grow together through increasing of (E) the mixing radius or (F) increasing durations of CO2 injection to the water table. (G) Dropping sea level places caves in the vadose zone and halts cave enlargement. In the vadose zone humid cave chambers promote the growth of speleothems. (H) Loss of buoyant support, denudation, and rock fatigue induce varying degrees of collapse, forming banana holes. Illustrations are based on concepts described in Harris et. al., (1995) and Gulley et. al., (2015).

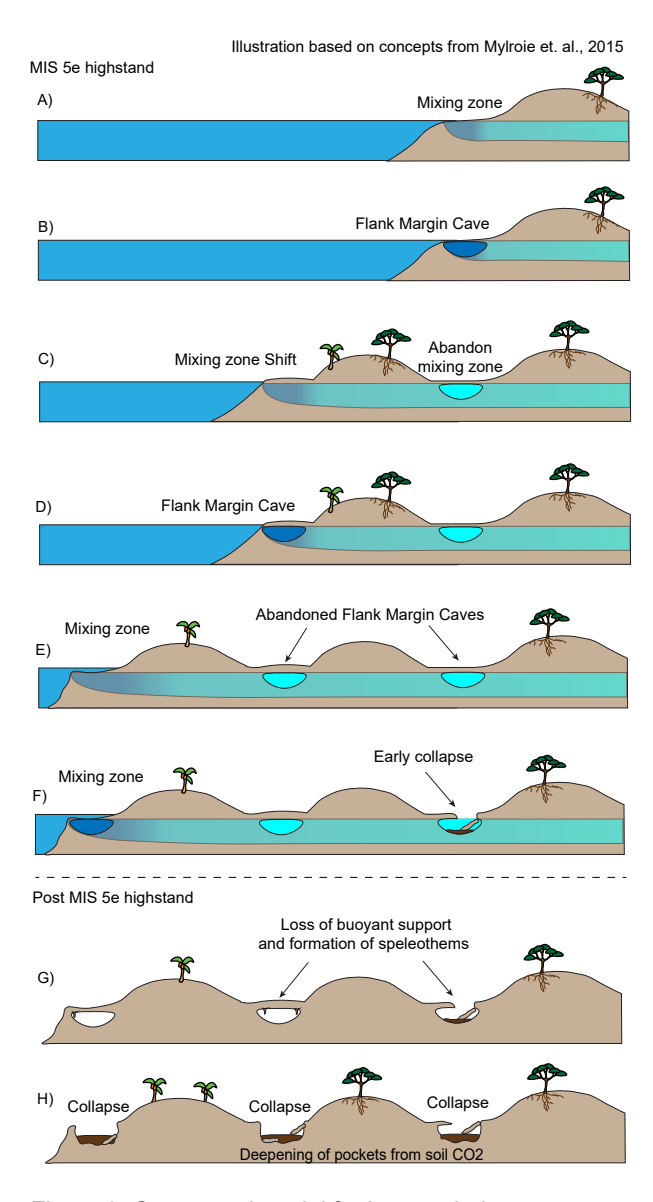


Figure 3: Conceptual model for banana holes as syndepositional flank margin caves forming within an advancing strand plain. (A) A freshwater lens invades newly deposited land pacing a mixing zone near the shoreface. (B) Pausing of the mixing zone at the shoreface drives dissolution, thereby creating a small flank margin cave. (C) Deposition of the next strandplain generation results in the mixing zone shifting, and thus, dissolution is halted in the original cave chamber and is initiated at the new shoreface. (D) The new mixing zone results in another immature flank margin cave. Continued progradation of the strand plain and episodic shifting of the mixing zone (E) creates multiple cave chambers advancing toward the shoreline. (F) Older generations of these caves may collapse as new caves are still forming. (G) Falling sea levels place cave chambers in the vadose zone where they accumulate speleothems before (H) collapsing to form banana holes. Illustrations are based on concepts described in Mylroie et. al., (2016).

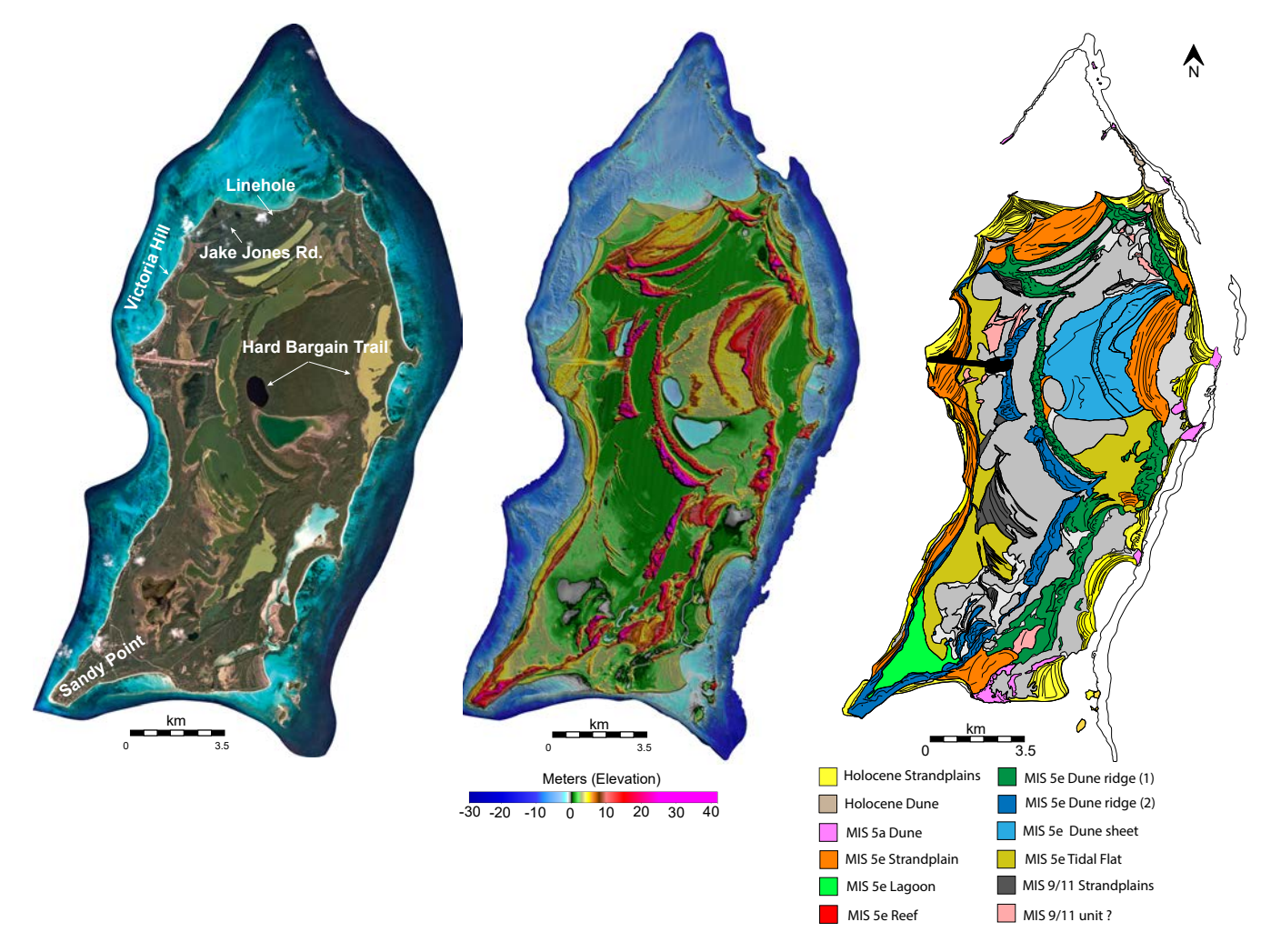


Figure 4: (A) Satellite photo from digital globe modified from Kerans et. al., 2018 (B) airborne LiDAR derived digital elevation model collected and processed by NCALM and (C) geologic map of San Salvador Island Bahamas modified from Kerans et. al (2018). Our study focuses on Holocene, MIS 5e and MIS 9/11 strand plains.

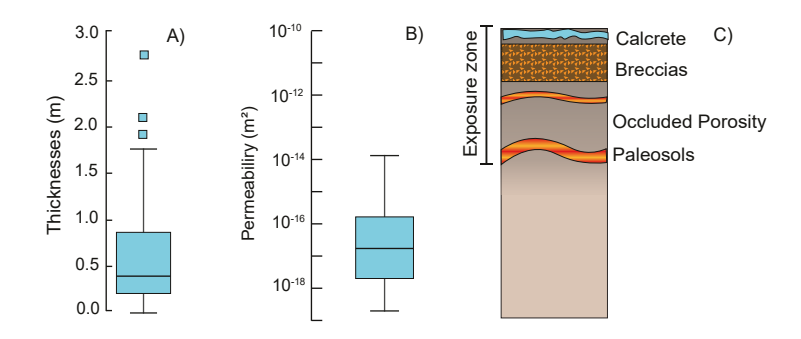


Figure 5: (A) Exposure zone thicknesses and (B) permeabilities from the Sandy Point region of San Salvador Island Bahamas. Diagram illustrating compositional elements commonly found in exposure zones. Exposure Zone Data From: Breithaupt 2020., Chapter 2

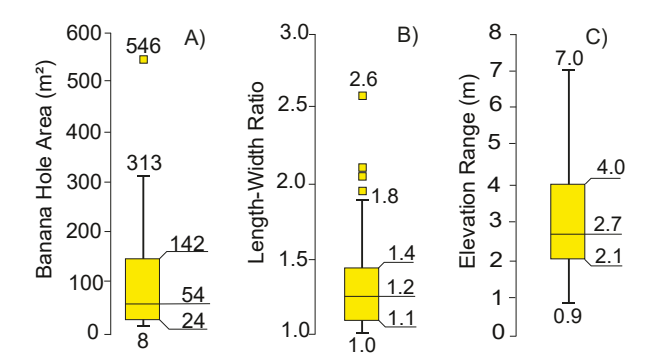


Figure 6: Field validated data from 71 banana holes near Line Hole well field, Jake Jones road, Hard Bargain, and Victoria Hill. (A) Banana hole areas, (B) length to width ratio, (C) and elevation ranges used to constrain LiDAR detections to banana hole morphologies. Field validated data from Infante et. al., (2012).

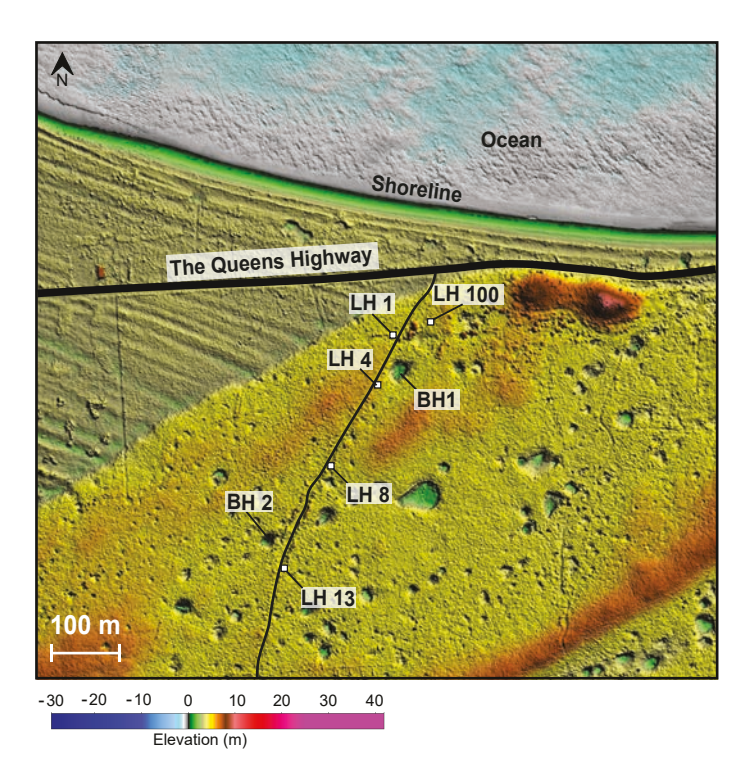


Figure 7: Location of sample sites at the Line Hole well field on the LIDAR derived digital elevation model. Hot colors represent higher elevations while cool colors represent lower elevations. We collected pressure records in each of the labeled locations over several trips. Several banana holes (similar to those labeled BH1 and BH2) are observed surrounding the sample locations. The floor elevations of banana holes are about 1-2 meters RSL (e.g. the color bar).

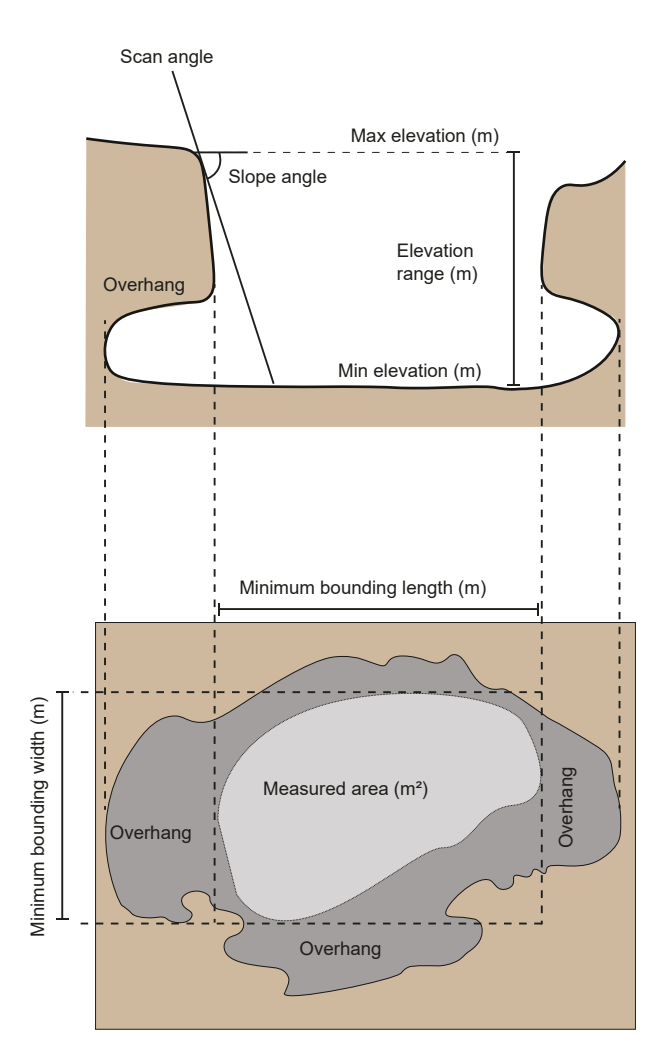


Figure 8: Illustration of parameters collected from banana holes and limitations of the LiDAR guided analysis of banana hole distributions. The maximum scan angle of the lidar is 60 degrees, however steeper slopes can be calculated when opposite side of depressions are intersected by the laser. The minimum elevation represents the floor of the banana hole, the maximum elevation represents the lip, and the elevation range represents the total thickness. The total thickness includes will overestimate the dissolutional cave height which is the distance between the floor and overhang. The minimum bounding length (MBL) and width are used to calculate minimum bounding area (MBA) of the banana hole. Banana hole areas correspond to the exposed floor area while portions under overhangs cannot be quantified with LiDAR data.

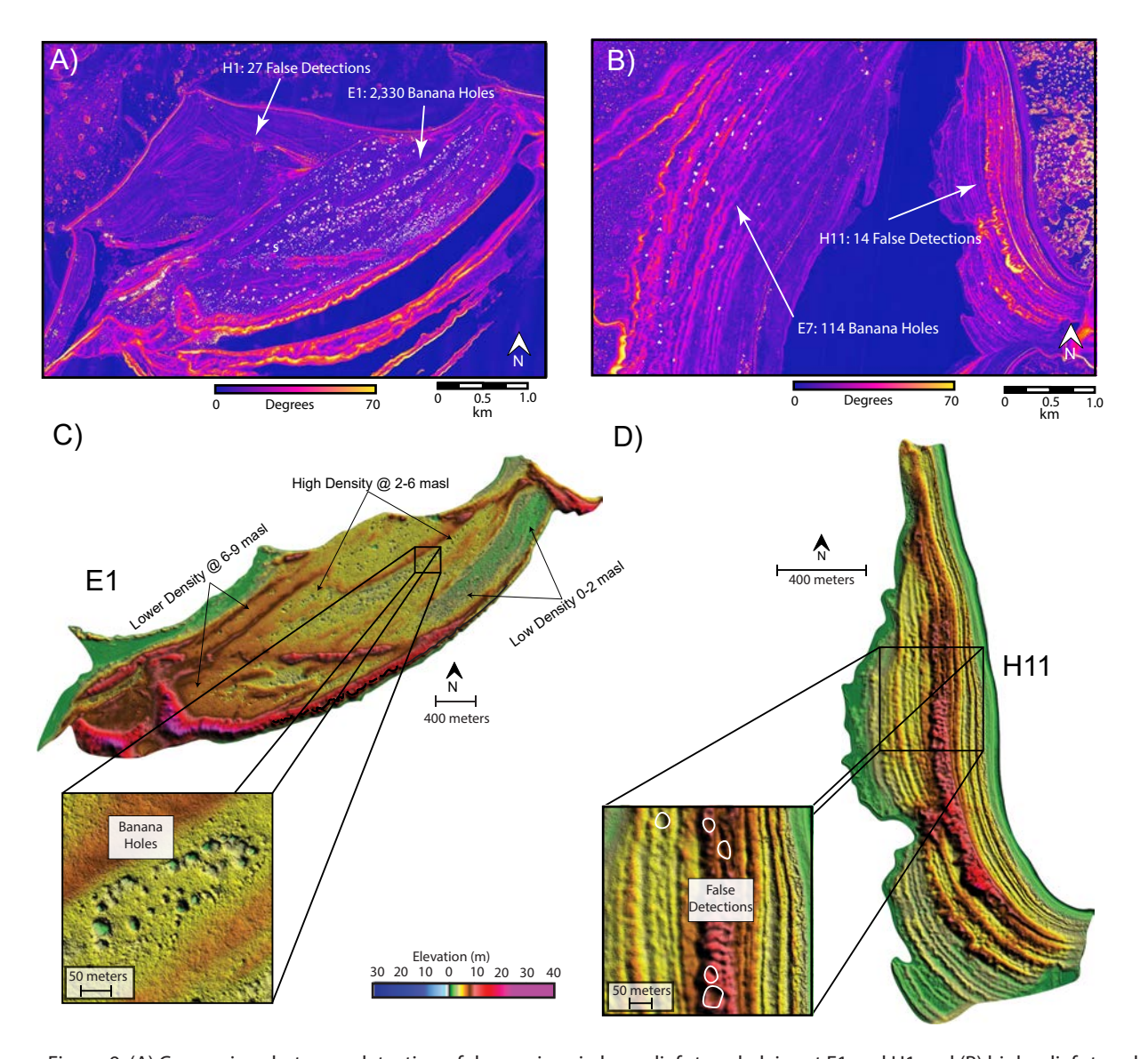


Figure 9: (A) Comparison between detection of depressions in low relief strand plains at E1 and H1 and (B) high relief strand plains at H7 and H11. A high density of banana holes were observed in (C) Pleistocene strand plains while all detections of depressions in (D) Holocene strand plains were determined to be false positives. Most false positives were due to anthropogenic enclosures, such as pools, pits and rubble piles, however, some natural dune morphology resulted in steep walled circular pits which were removed manually given their similarity to the filtering scheme.

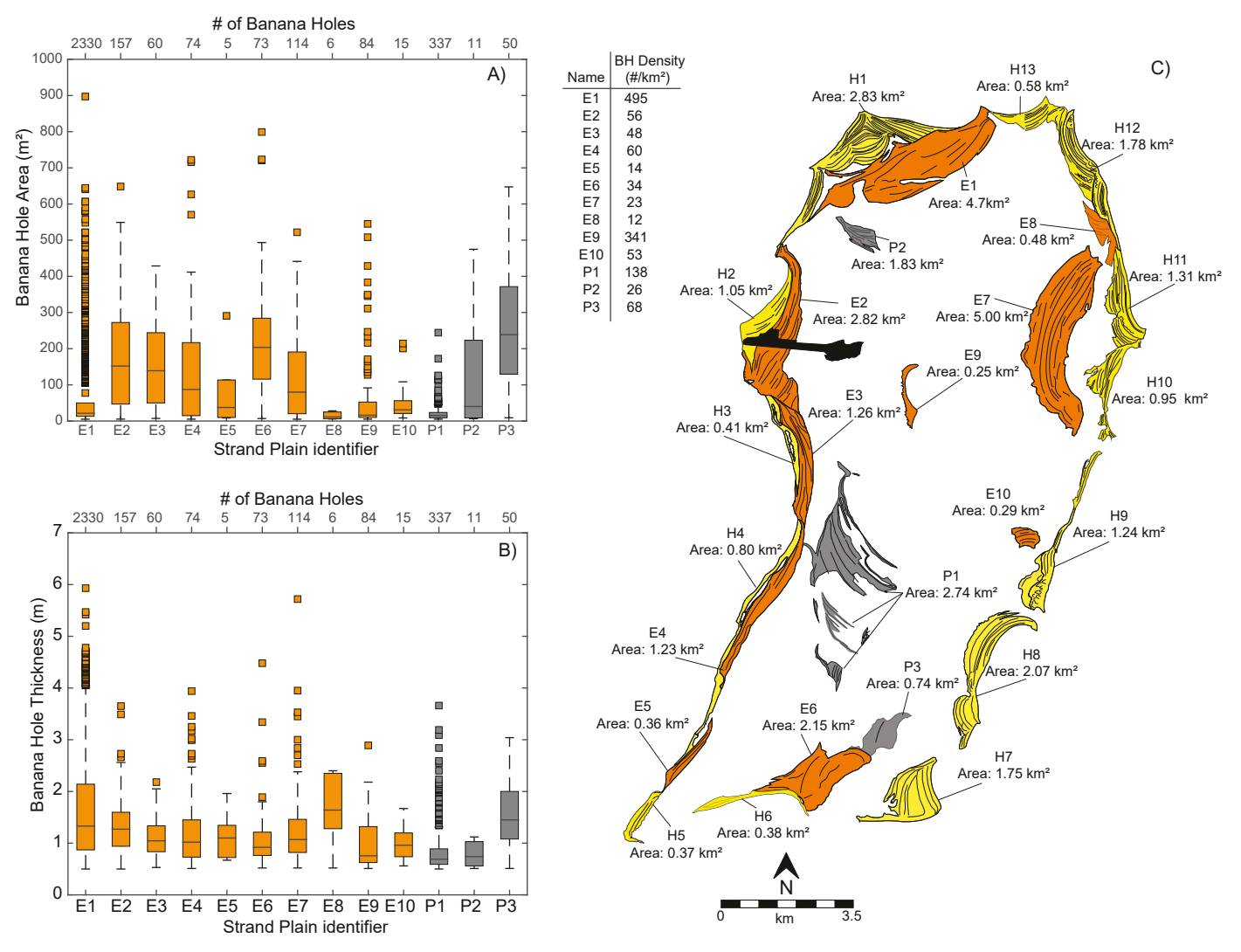


Figure 10: Summary of (A) area, (B) elevation range (thickness) and (C) densities of banana holes by strand plain. Yellow polygons represent Holocene strandplains, orange represent MIS 5e strandplains and gray represent MIS 9/11 strandplains. Note the large number of outliers in E1 which has the highest karst density of all strand plains on San Salvador island. All box plots use a different sample population based on their strand location. BH = Banana Hole.

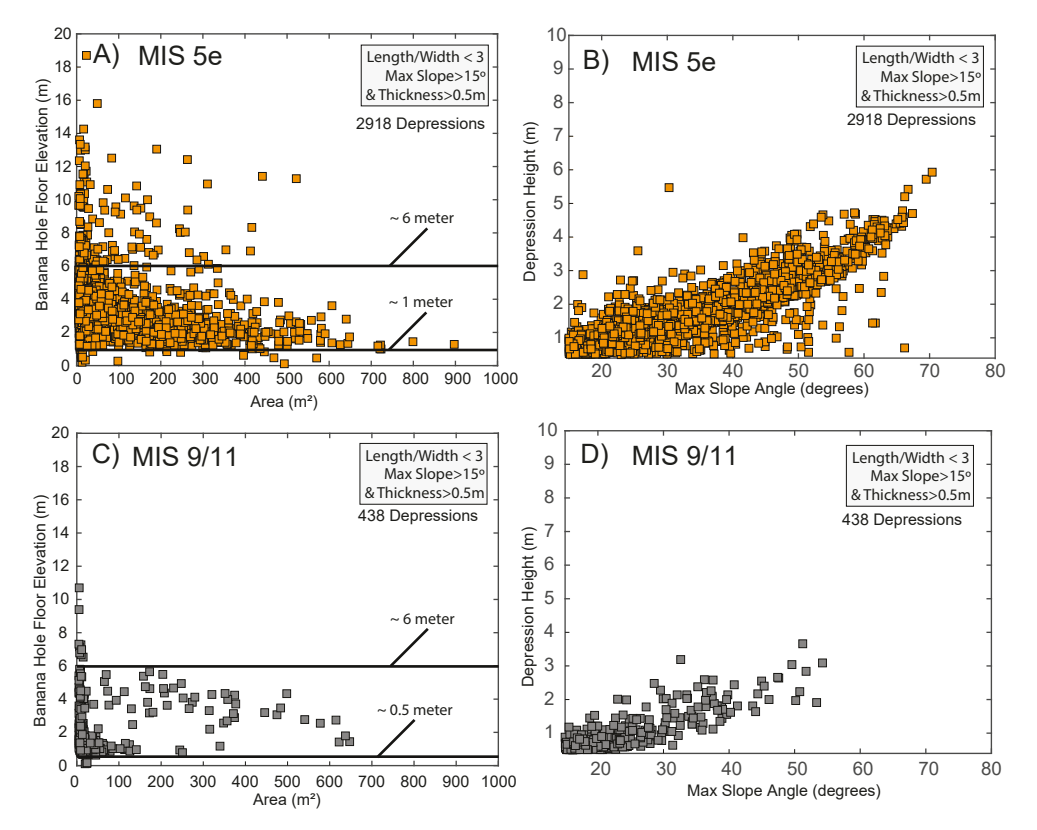


Figure 11: (A) Elevation of MIS 5e bananā hole floors vs area and (B) banana hole elevation range vs. maximum slope angle. (C) Elevation of MIS9/11 banana hole floors vs area and (D) banana hole elevation range vs. maximum slope angle. See Figure 8 for key to measurement types. Banana hole floors are observed above 6 meters elevation in MIS 5e strand plains and thus could not have formed at past water tables. We observe a large number of banana hole floors which are between 1 and 6 meters RSL but very few below 1 meter suggesting a possible horizon or contact controlling banana hole elevations. High slope angles in banana holes likely represent more recently collapsed pits while shallower angles represent banana holes which have undergone denudation thereby reducing their slope angles as pits partially fill in. The impact of denudation can be observed between MIS 5e and MIS 9/11 banana given the general shallowing of banana holes with time. The post-collapse down wasting has likely removed many banana holes from the MIS9/11 surface or made them undetectable due to infilling. Thus, the density of MIS 9/11 banana holes is likely underestimated.

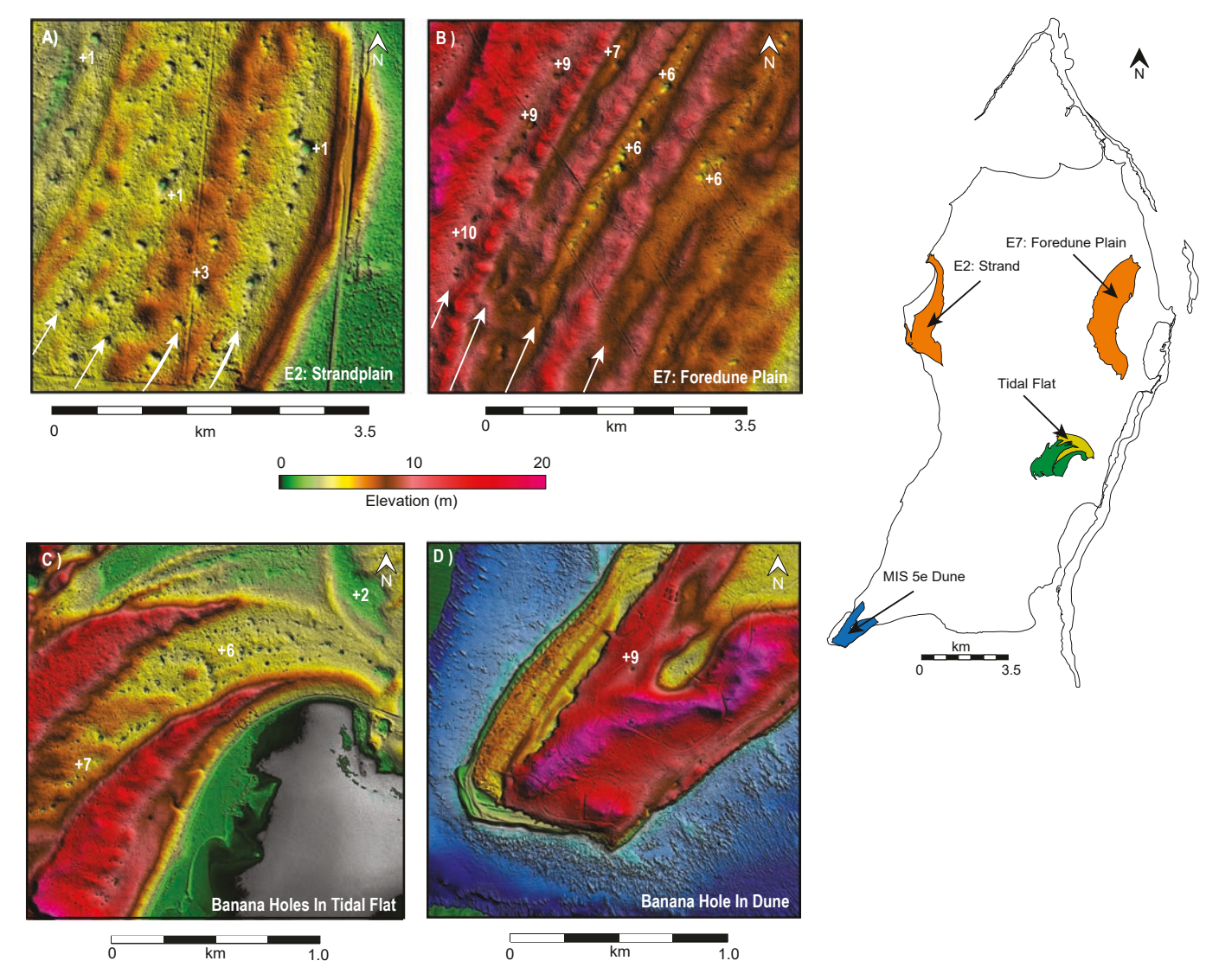


Figure 12: (A) Examples of banana holes observed in the E2 Strandplain (B) the E7 foredune plain, (C) tidal flat facies, and (D) dune facies. The elevations of several banana hole floors (white numbers) are above the +6 meter sea level elevation reported for the MIS 5e highstand and thus could not have formed in the MIS 5e freshwater lens.



Figure 13: Satellite images of banana holes in the Line Hole strand plain during (A) wet and (B) dry seasons. During wet seasons banana holes become almost entirely filled with rainwater while they are usually empty during the dry seasons. Elevations near the tops of banana holes are between 4 and 5 meters above sea level, and thus, water levels must be elevated above the rest of the water table.

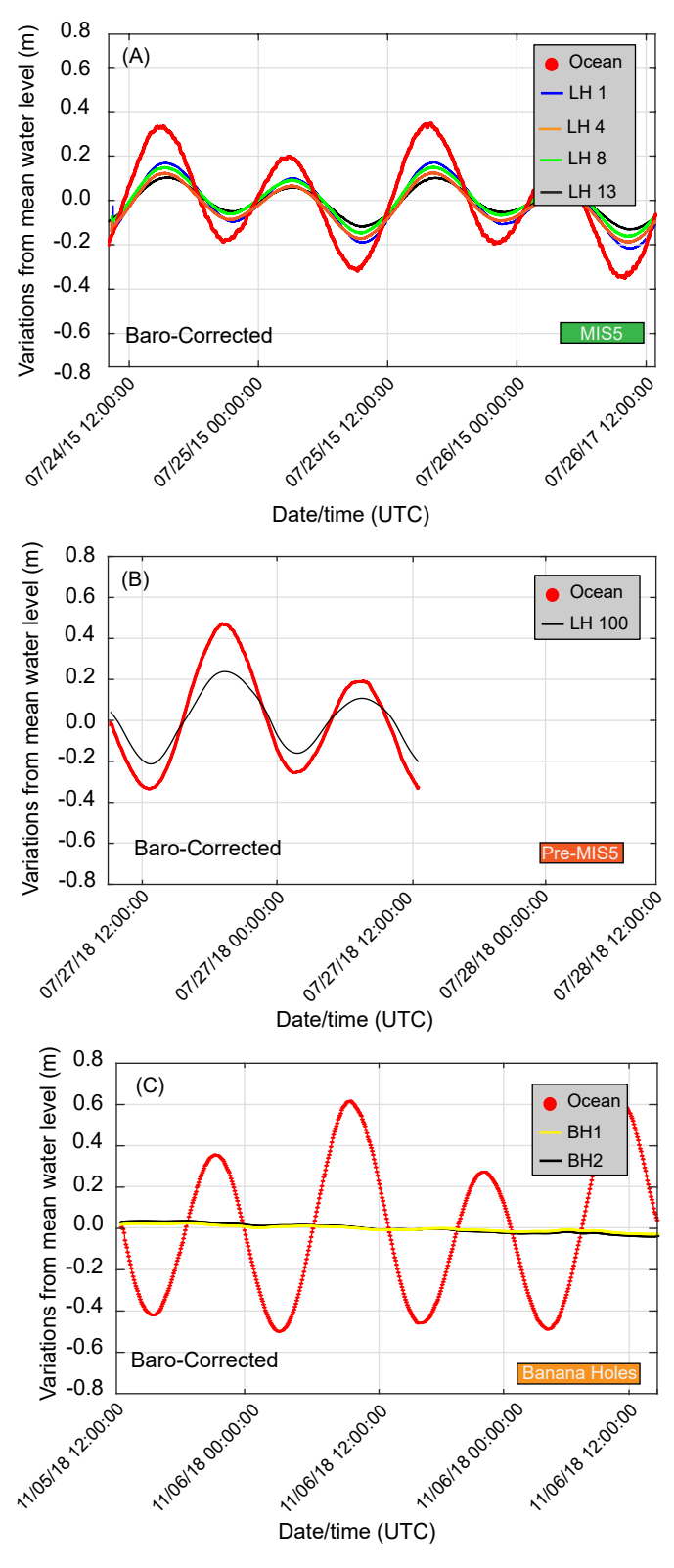


Figure 14: Tidal records in the Line hole well field (A), LH-Deep (B), and two banana holes (C). Strong tidal periodicity is observed in the Line Hole wells and LH-Deep, yet, no tidal signal is observed in BH1 or BH2. We suggest the lack in tidal periodicity indicates the banana holes are disconnected from the underlying aquifer. The decrease in water level in BH1 and BH2 indicate slow drainage of water from the banana hole across the perching interface.

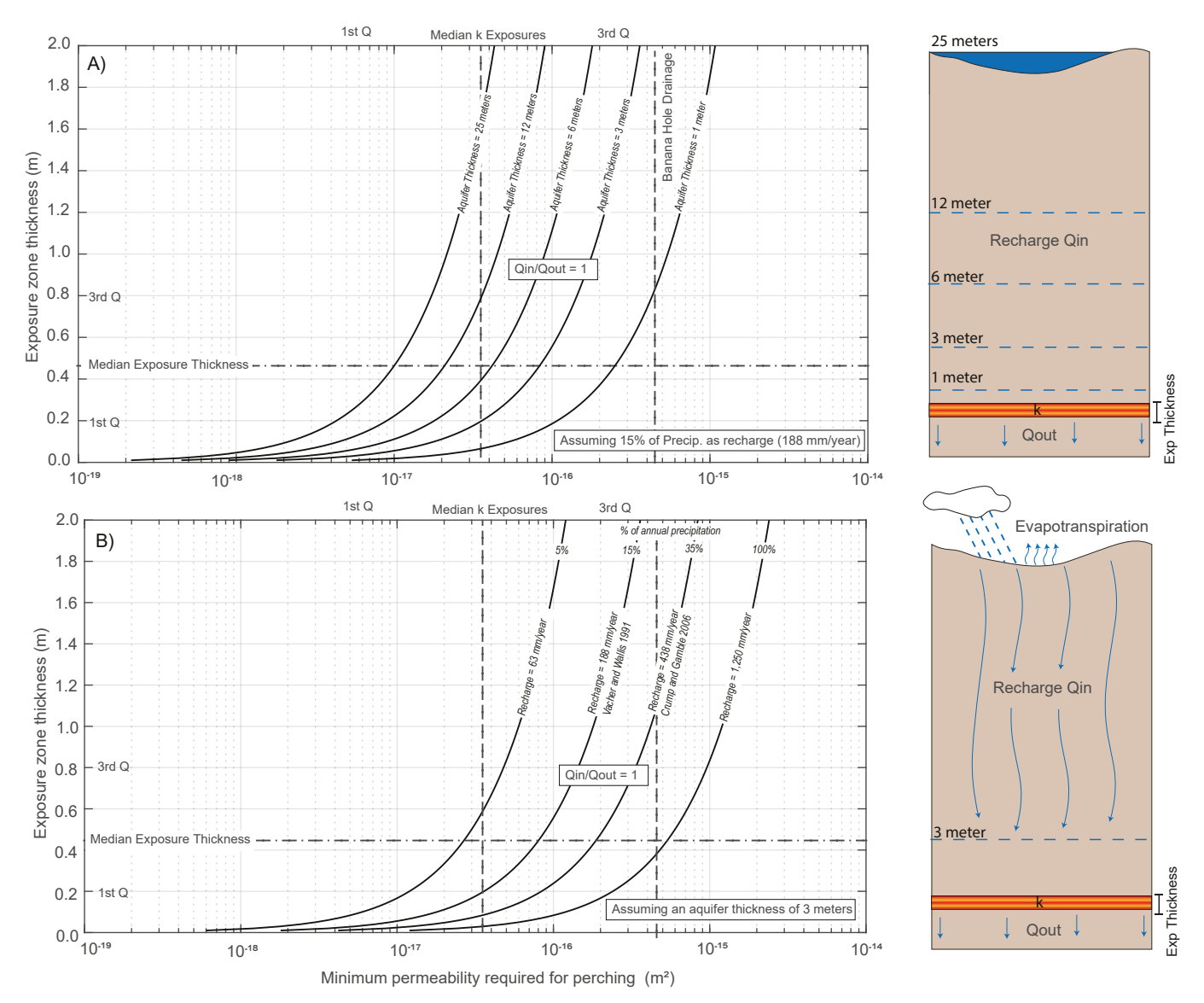


Figure 15: One dimensional perched aquifer model assuming no lateral flow and constant head. (A) Estimates for exposure surface thickness and permeabilities required to maintain perched aquifers between 1 and 25 meters assuming a constant recharge of 188 mm/year or 15% of annual precipitation. (B) Estimates of exposure thickness and permeability required to maintain an aquifer 3 meters in thickness for varying recharge magnitudes. We include the 1st quartile, median and 3rd quartile values for exposure surface thickness and permeabilities as measured from core plugs and core descriptions (Breithaupt 2020, Chapter 2). Recharge between 15 and 35% of annual precipitation have been estimated for islands such as San Salvador (Crump and Gamble, 2006) and Exuma (Vacher and Wallis 1991) and are used to bracket the likely magnitudes.

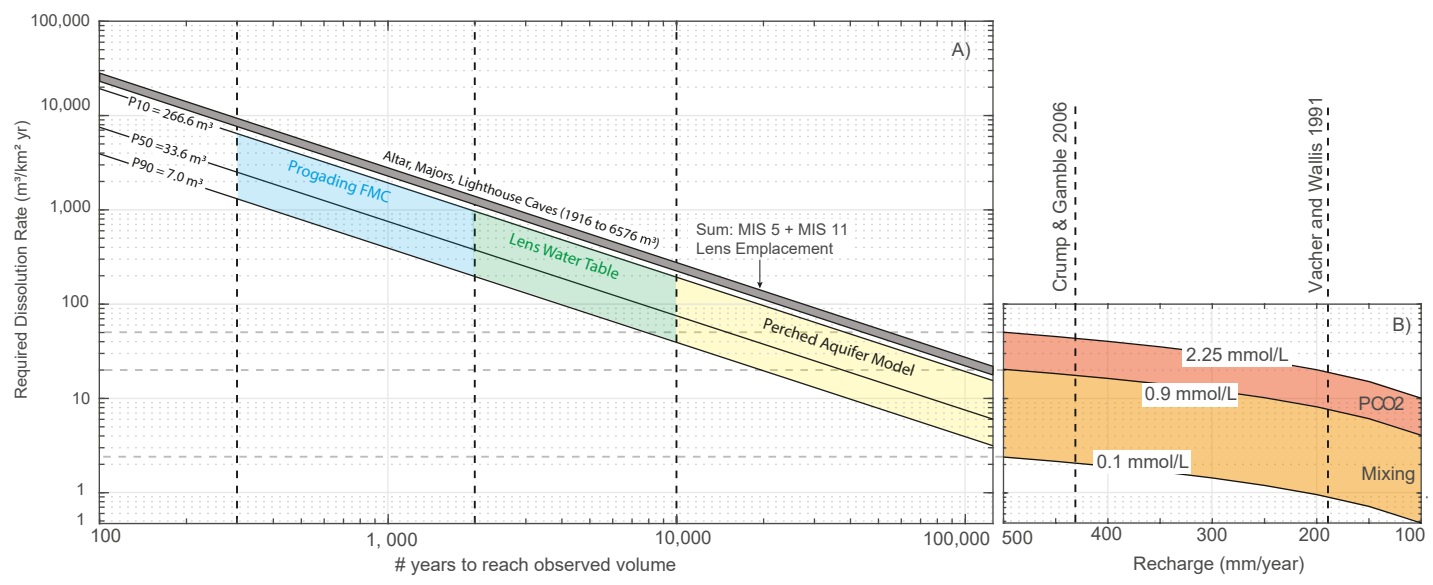


Figure 16: (A) Dissolution rates estimated given different time-frames for banana hole and flank margin cave formation on San Salvador Island. The dissolution rate is calculated for the P90, P50, and P10 of 2918 banana hole volumes in MIS 5e bedrock. We also estimate dissolution rates for the three largest flank margin caves (Altar, Majors and Lighthouse) in both MIS 5e and MIS9/11 bedrock. Dissolution rates required to create banana holes in a prograding strand plain are highlighted in blue, within the freshwater lens during MIS 5e are highlighted in green, and in perched aquifers are highlighted in yellow. The gray shaded area represents dissolution rates for Altar, Major's and Lighthouse caves, while the arrow shows the cumulative time frame freshwater lenses could have occupied MIS 9/11 bedrock and the corresponding dissolution rate required to create Majors and Lighthouse caves. (B) Dissolution rates derived from excess Ca2+ in water samples on San Salvador plotted against recharge. Excess Ca2+ values are from published data in the Sandy Point and Line hole well fields (Gulley et al., 2015) and recharge rates are bracketed from previously published values (e.g. Vacher and Wallis 1991 and Crump and Gamble (2006)). Dissolution rates required to create banana holes in 300 to 2000 years (progradational FMC model) are about 2 orders of magnitude greater than values calculated from both heterogeneous PCO2 and mixing models. Banana holes forming between 2 and 10 thousand years require dissolution rates an order of magnitude greater than those from heterogeneous PCO2 and mixing models. Only the perched aquifer model yields dissolution rates consistent with models calibrated to measured excess Ca2+ in San Salvador.

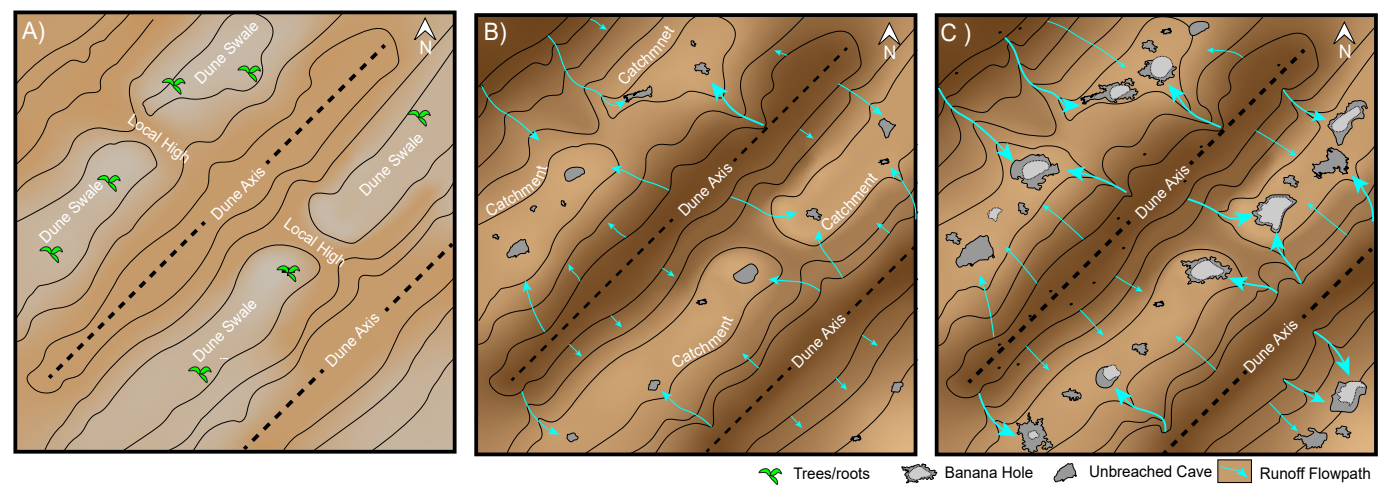


Figure 17: Map view conceptualization of topographic controls on banana hole formation. (A) Strand plains are deposited on the platform. Due to high matrix porosity and lack of surface induration, meteoric waters rapidly infiltrate though the matrix porosity, and little runoff is focused to topographic lows. (B) Calcretes and paleosols begin developing immediately after bedrock deposition as cementation creates indurated surfaces. Over longer durations of exposure, thick calcretes and paleosols form. Indurated crusts on the land surface allow recharge to flow to catchments between ridges, where heterogeneities deliver aragonite and calcite undersaturated waters to the subsurface driving void formation. (C) Voids initially are completely enclosed beneath the land surface, forming large single chambered caves before collapse. Continued denudation and weathering result in more collapse over time and once open to the atmosphere banana holes accumulate soils.

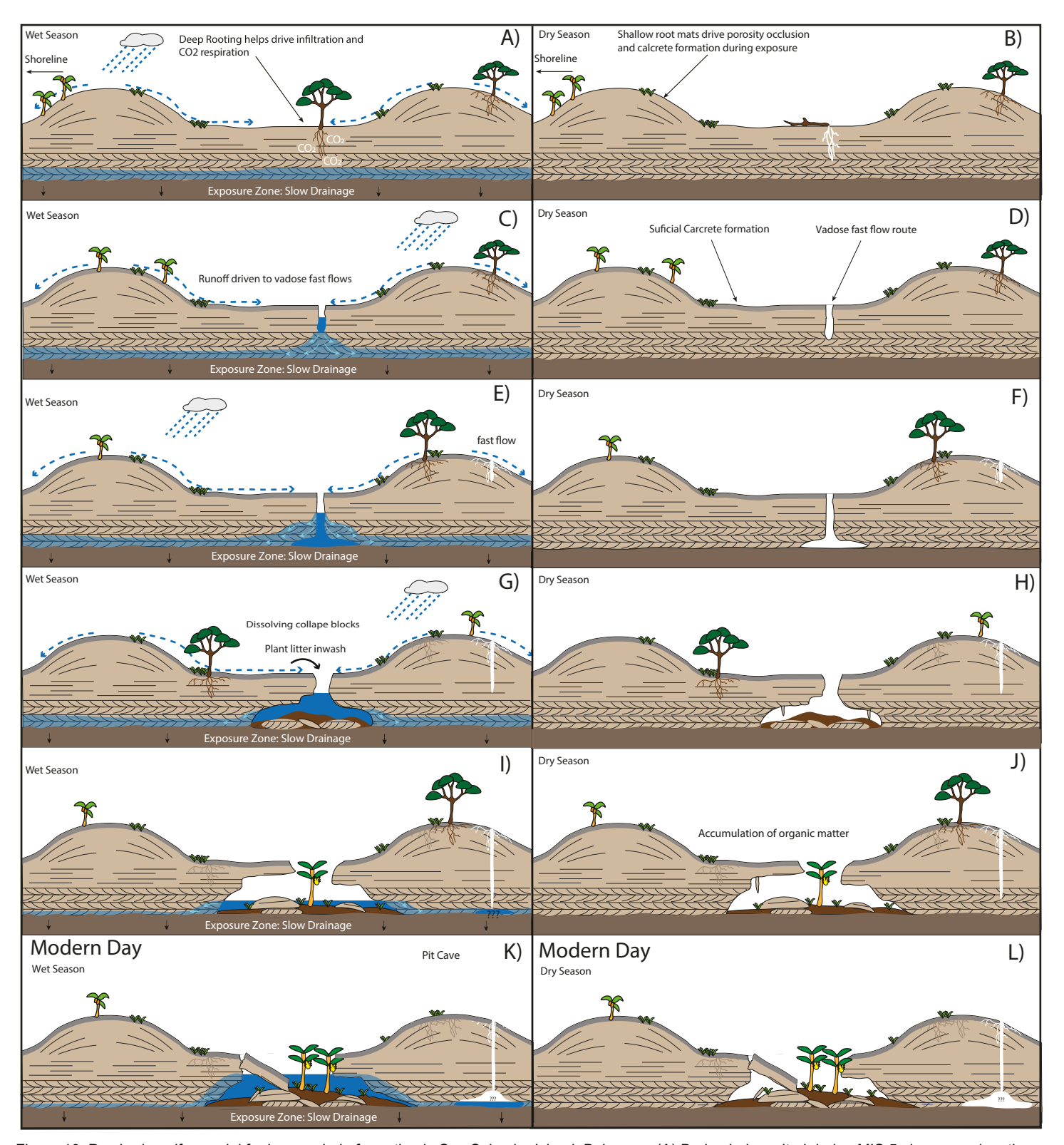


Figure 18: Perched aquifer model for banana hole formation in San Salvador Island, Bahamas. (A) Bedrock deposited during MIS 5e is exposed on the platform entering the low stand. (B) Initial formation of heterogeneities in the topographic lows are driven by fracturing and roots boring through bedrock to ephemerally perched water tables. (C) Regular exposure to meteoric recharge causes surficial calcretes and paleosols to form on the land surface, driving runoff to topographic lows where infiltration occurs through high permeability matrix porosity, fractures, and root casts. (D) Preferred pathways for recharge are dissolutionally enlarged by descending waters, and progressively deepen with each rainfall event. until intersecting a permeability interface. (E) As waters intersect the low permeability surface, they are forced laterally along the interface thereby under-cutting bedrock and resulting in thin lateral chambers above the permeability interface. (F) During dry seasons, waters slowly drain across the surface and dissolution ceases, and thin chambers become air-filled. (G) Repeated filling and draining cycles result in thin, laterally extensive chambers, which begin to collapse due to wide spans thereby vertically migrating the void space. Collapse blocks may become encased in organic rich soils which act to increase CO2 concentrations and more efficiently dissolve blocks during filling and draining cycles. H) Air filled chambers may grow speleothems depending on their roof and walls. (I) Continued collapse begins to expose voids to the atmosphere allowing larger vegetation to grow in organic rich soils. (J) Pit caves which had been forming simultaneously, yet at a slower rate due to lower runoff volumes, begin to reach the low permeability interface and enlarge voids. (K) Modern day banana holes have overhung to collapsed roofs, contain soil mats in their floors, and of course, often contain banana trees. (L) During modern wet seasons, banana holes become filled with waters perched on permeability bounda